Quantifying co-seismic and post-seismic slip on fault scarps and their erosional modification using high-resolution Pleiades optical satellite data and repeat Terrestrial Laser Scanning: the 2016 Mw 6.6 Norcia earthquake (Central Italy)

ROBERT GILES ELLIOTT

Appendices

Table of Contents

APPENDIX 3A

3A1. Model fault geometry

Table 3A Fault Geometry used in slip inversion

Strike	Dip	Rake	Easting/1000	Northing/1000	length	surface	depth	patch1	patch2	ID
158	40	-135	349.700	4757.000	12	0	5	12	5	1
158	40	-45	349.700	4757.000	12	0	5	12	5	2
155	40	-135	350.000	4759.000	16	0	5	16	5	3
155	40	-110	355.085	4749.320	6.4	0	10	13	20	3
185	45	-80	356.377	4746.070	0.75	0	10	3	40	3
177	45	-88	356.400	4744.600	2.2	0	10	10	40	3
158	45	-127	356.560	4743.260	1.45	0	10	6	40	3
138	45	-147	357.420	4741.900	1.8	0	10	8	40	3
170	40	-135	358.550	4738.200	6.2	0	10	12	20	3
155	40	-45	350.000	4759.000	16	0	5	16	5	4
155	40	-20	355.085	4749.320	6.4	0	10	13	20	4
185	45	10	356.377	4746.070	0.75	0	10	3	40	4
177	45	2	356.400	4744.600	2.2	0	10	10	40	4
158	45	-37	356.560	4743.260	1.45	0	10	6	40	4
138	45	-57	357.420	4741.900	1.8	0	10	8	40	4
170	40	-45	358.550	4738.200	6.2	0	10	12	20	4
133	65	-132	356.370	4743.270	0.4	0	3	2	12	5
170	65	-95	356.620	4742.800	0.65	0	3	3	12	5
205	65	-60	356.590	4742.320	0.4	0	3	2	12	5
168	50	-95	357.400	4737.966	8.5	0	3	17	6	5
133	65	-42	356.370	4743.270	0.4	0	3	2	12	6
170	65	-5	356.620	4742.800	0.65	0	3	3	12	6
205	65	30	356.590	4742.320	0.4	0	3	2	12	6
168	50	-5	357.400	4737.966	8.5	0	3	17	6	6

330	70	-165	356.950	4741.500	2	0	2	16	16	7
335	70	-165	356.520	4742.600	0.3	0	2	1	4	7
330	70	-75	356.950	4741.500	2	0	2	16	16	8
335	70	-75	356.520	4742.600	0.3	0	2	1	4	8
320	40	-165	353.090	4747.300	6	0	2	6	2	9
320	40	-75	353.090	4747.300	6	0	2	6	2	10
354	70	-135	350.930	4735.280	9	0	10	9	10	11
354	70	-45	350.930	4735.280	9	0	10	9	10	12
222	40	-102	354.246	4734.740	9	0	8	9	8	13
222	40	-12	354.246	4734.740	9	0	8	9	8	14
163	45	-135	360.850	4726.660	15	0	10	15	10	15
163	45	-45	360.850	4726.660	15	0	10	15	10	16
118	45	-157	357.750	4741.060	0.7	0	3	3	12	17
118	45	-67	357.750	4741.060	0.7	0	3	3	12	18

3A2. Comparison with fit to data and slip vectors for a model with 14 fault segments.

Dataset	Weighting	RMS misfit sf 150	sf 150/weighting	RMs misfit alt geom	alt geom/weighting	% increase in misfit using alt geom
Pleiades EW	1.00000	0.13993	0.13993	1.41082	0.14108	1%
Pleiades NS	1.00000	0.14378	0.14378	1.45838	0.14584	1%
Pleiades vertical	1.00000	0.18226	0.18226	1.85686	0.18569	2%
ALOS	3.00000	0.04641	0.01547	0.04710	0.01570	1%
Sentinel	3.00000	0.03924	0.01308	0.03977	0.01326	1%
Relative GNSS EW	5.00000	0.23827	0.04765	0.25333	0.05067	6%
Relative GNSS NS	5.00000	0.21941	0.04388	0.25298	0.05060	15%
Relative GNSS vertical	5.00000	0.34553	0.06911	0.36566	0.07313	6%
Far-field GNSS EW	5.00000	0.06107	0.01221	0.06389	0.01278	5%
Far-field GNSS NS	5.00000	0.03111	0.00622	0.03271	0.00654	5%
Far-field GNSS vertical	5.00000	0.03426	0.00685	0.03440	0.00688	0%

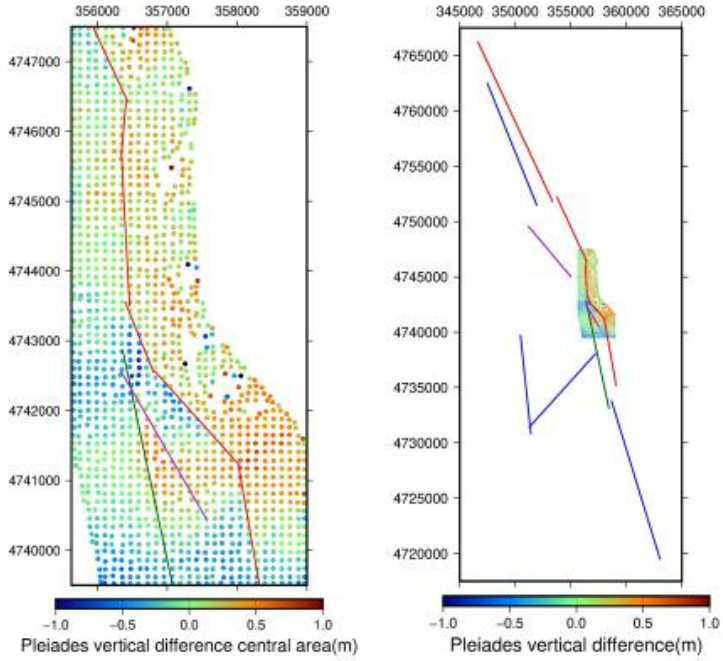

Figure 3A1 Alternative model fault geometry using 14 fault segments, detail in Pleiades data area (LH panel) and in far-field area (RH panel)

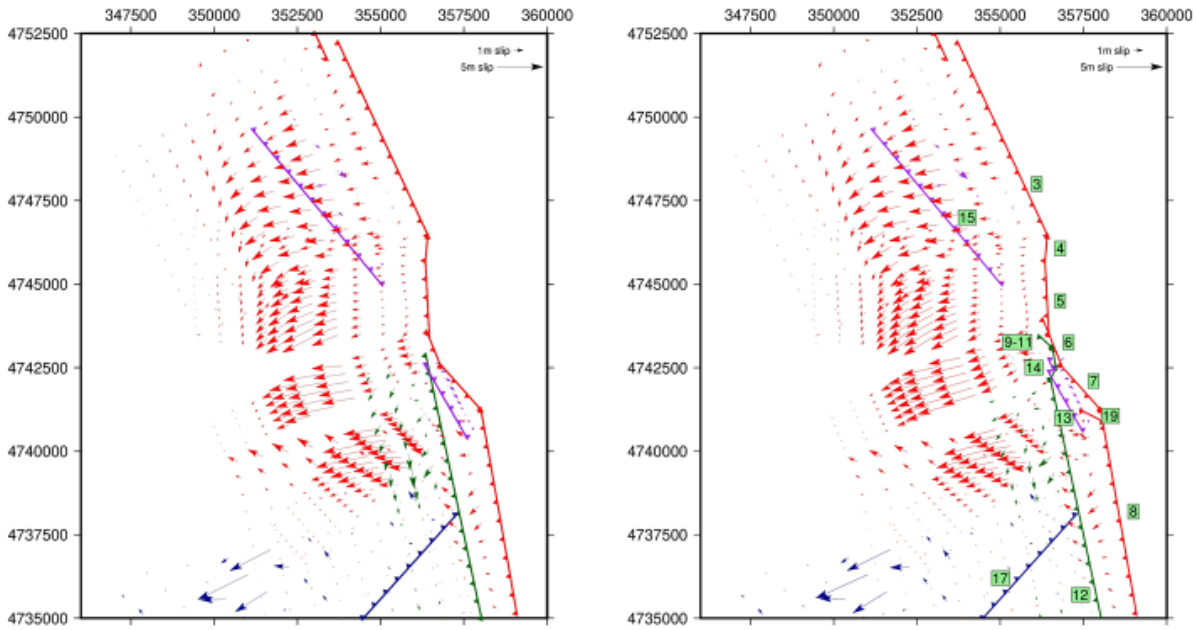

Figure 3A2, Comparison of modified central geometry of alternative 14 fault model (LH panel) compared to 19 fault model (RH panel), with resulting slip vectors from respective modelling down-sampled to ~ 0.5 km x 0.5 km

3A3. Comparison outputs by individual fault segments using differing smoothing factors.

(a) Smoothing factor 100

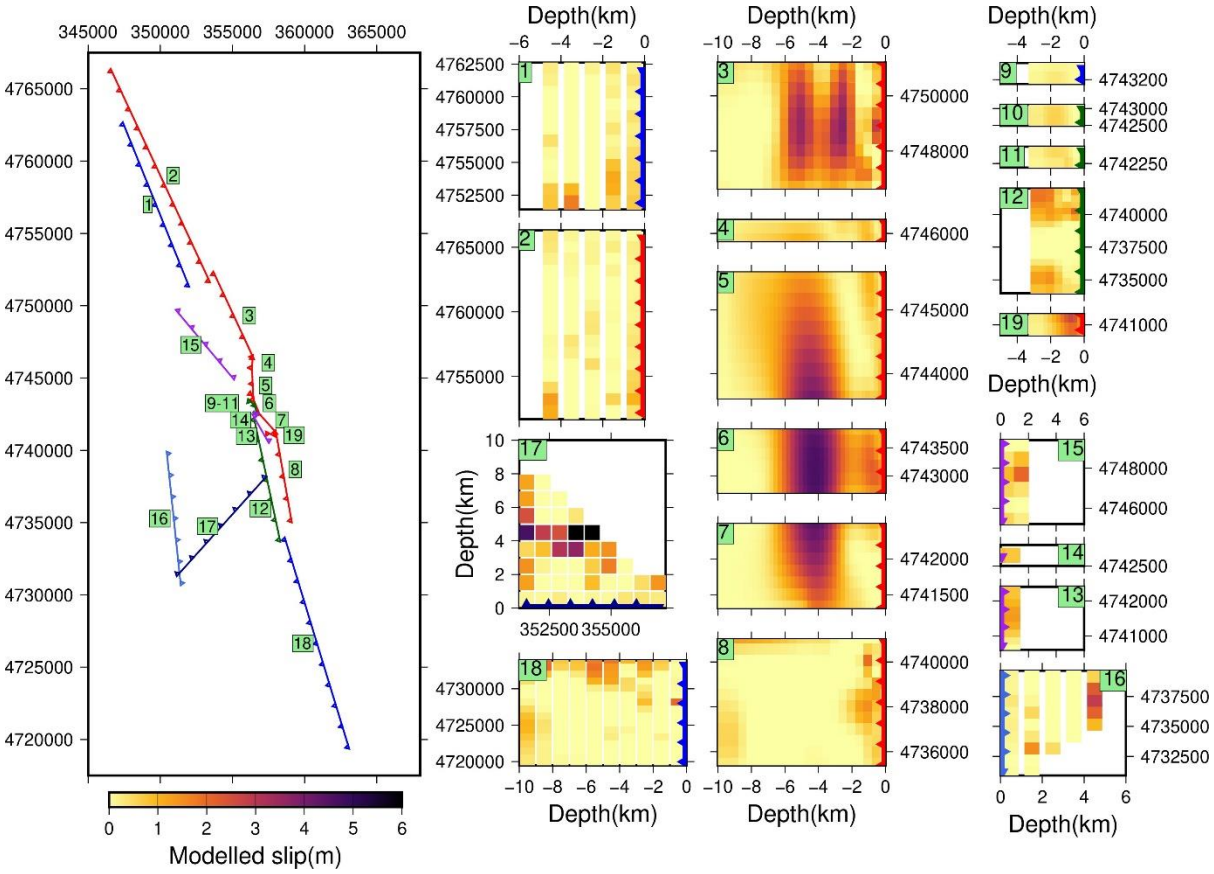

Figure 3A3 Results of joint inversion showing slip on individual fault segments by discretised patch. Location of the surface in each case is shown by a thicker line, with ticks showing dip direction. The numbers of each individual fault segment correspond to the locations shown on the plan figure (LH panel). Here, smoothing factor used was 100.

(b) Smoothing factor 150

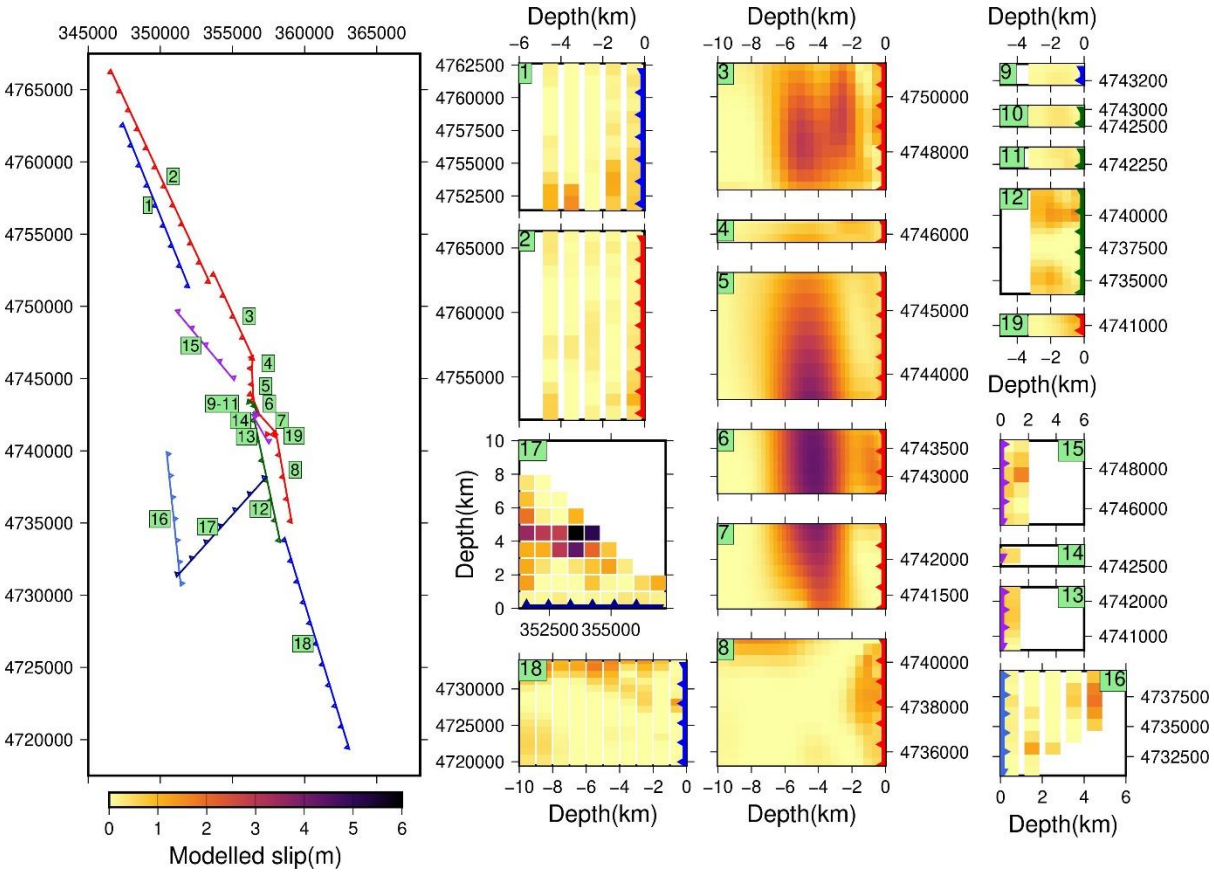

Figure 3A4 Results of joint inversion showing slip on individual fault segments by discretised patch. Location of the surface in each case is shown by a thicker line, with ticks showing dip direction. The numbers of each individual fault segment correspond to the locations shown in the plan figure (LH panel). Here, smoothing factor used was 150.

(c) Smoothing factor 200

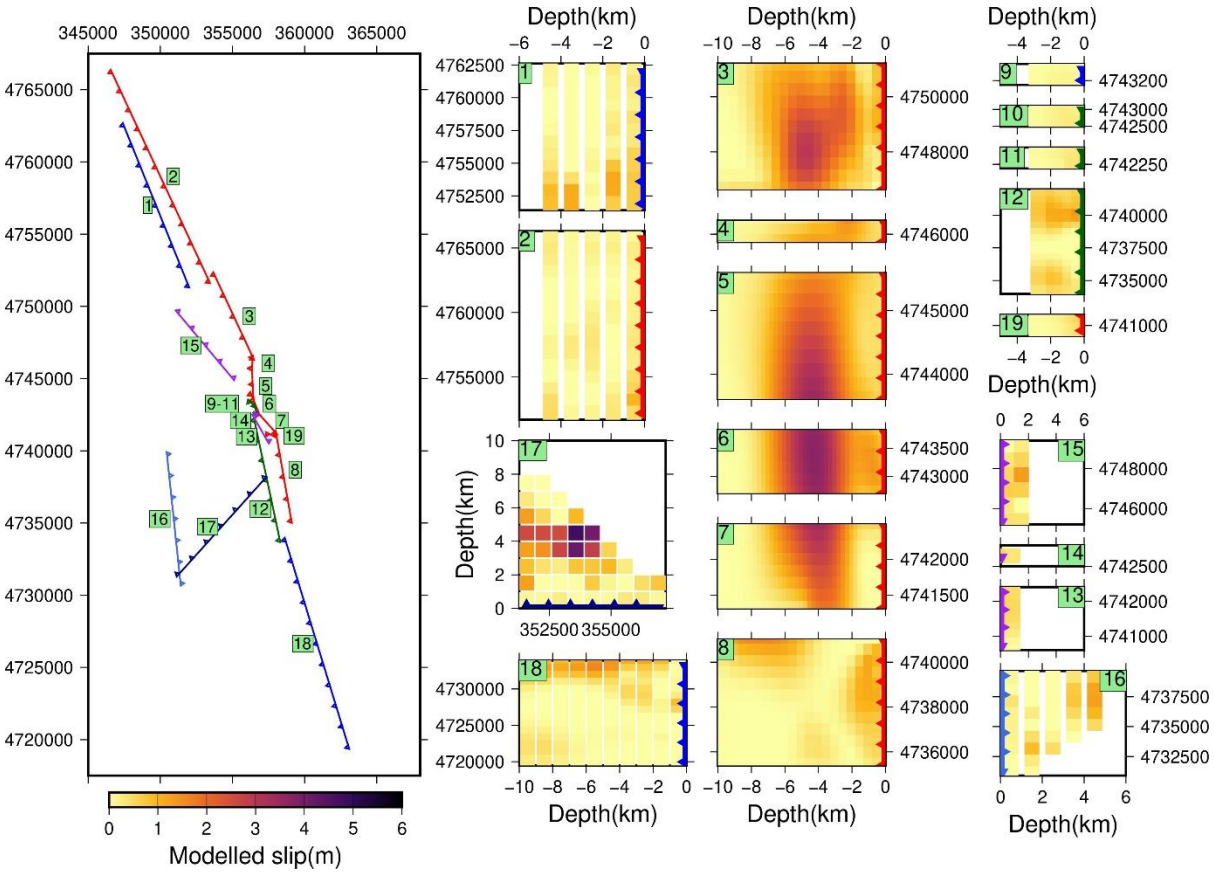

Figure 3A5 Results of joint inversion showing slip on individual fault segments by discretised patch. Location of the surface in each case is shown by a thicker line, with ticks showing dip direction. The numbers of each individual fault segment correspond to the locations shown in the plan figure (LH panel). Here, smoothing factor used was 200.

3A4.Table of RMS misfit values by smoothing factor

Dataset	Weight	RMS misfit sf 50	RMS misfit sf 100	RMS misfit sf 150	RMS misfit sf 200	sf 50/ weighting	sf 100/ weighting	sf 150/ weighting	sf 200/ weighting
Pleiades EW	1	0.13869	0.13899	0.13993	0.14189	0.13869	0.13899	0.13993	0.14189
Pleiades NS	1	0.14024	0.14168	0.14378	0.14533	0.14024	0.14168	0.14378	0.14533
Pleiades vertical	1	0.16691	0.17533	0.18226	0.18751	0.16691	0.17533	0.18226	0.18751
ALOS	3	0.04595	0.04505	0.04641	0.04845	0.01532	0.01502	0.01547	0.01615
Sentinel	3	0.03961	0.03862	0.03924	0.04028	0.01320	0.01287	0.01308	0.01343
Relative GNSS EW	5	0.14400	0.19042	0.23827	0.25633	0.02880	0.03808	0.04765	0.05127
Relative GNSS NS	5	0.25177	0.23595	0.21941	0.20681	0.05035	0.04719	0.04388	0.04136
Relative GNSS vertical	5	0.22514	0.28290	0.34553	0.38084	0.04503	0.05658	0.06911	0.07617
Far-field GNSS EW	5	0.05671	0.05849	0.06107	0.06428	0.01134	0.01170	0.01221	0.01286

Appendix 3A

Far-field GNSS NS	5	0.02678	0.02693	0.03111	0.03676	0.00536	0.00539	0.00622	0.00735
Far-field GNSS vertical	5	0.03609	0.03433	0.03426	0.03513	0.00722	0.00687	0.00685	0.00703

3A5. Slip vectors of individual fault segments

Fault 1 Monte Vettore N/synthetic

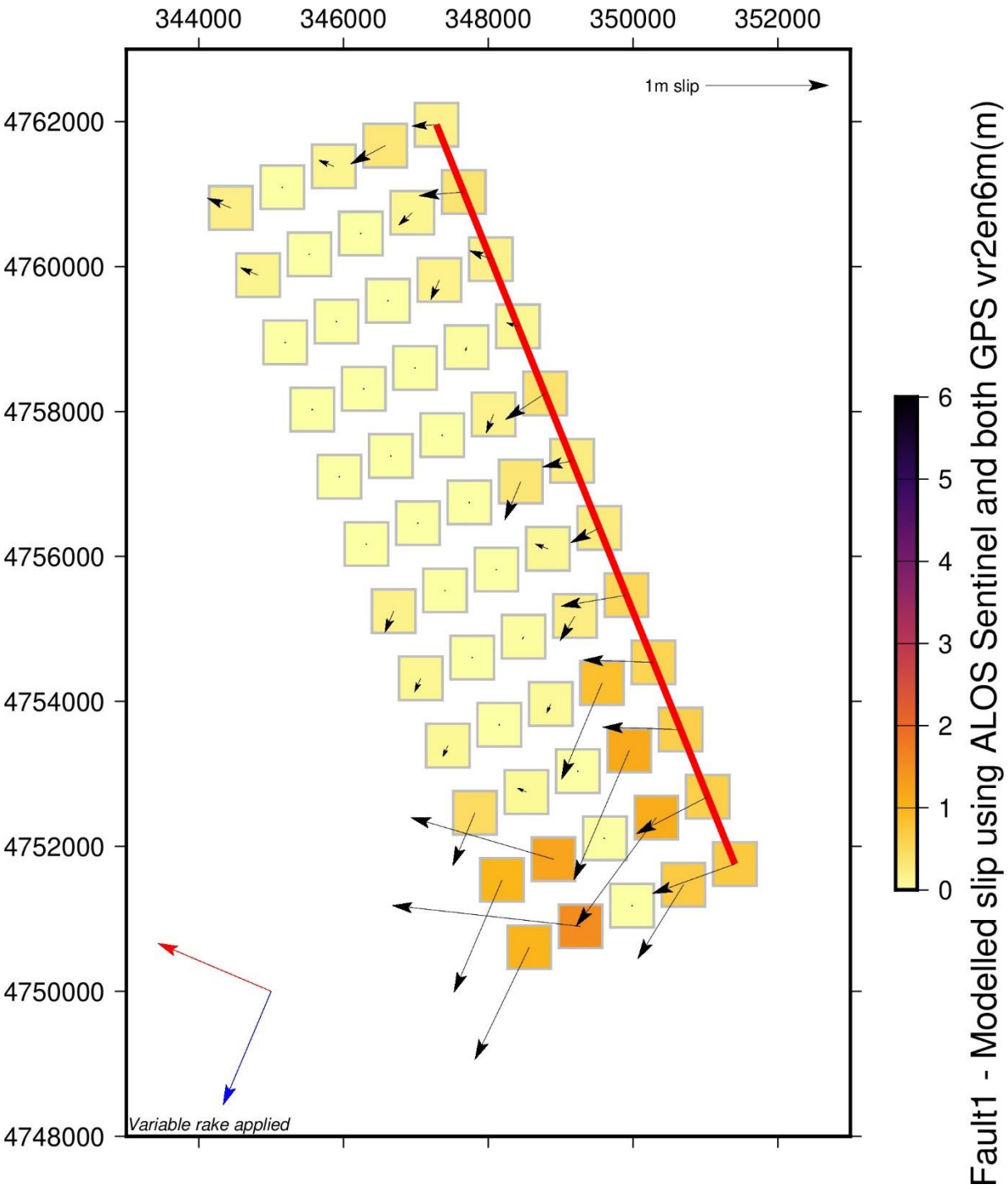

Fault 2 Monte Vettore N

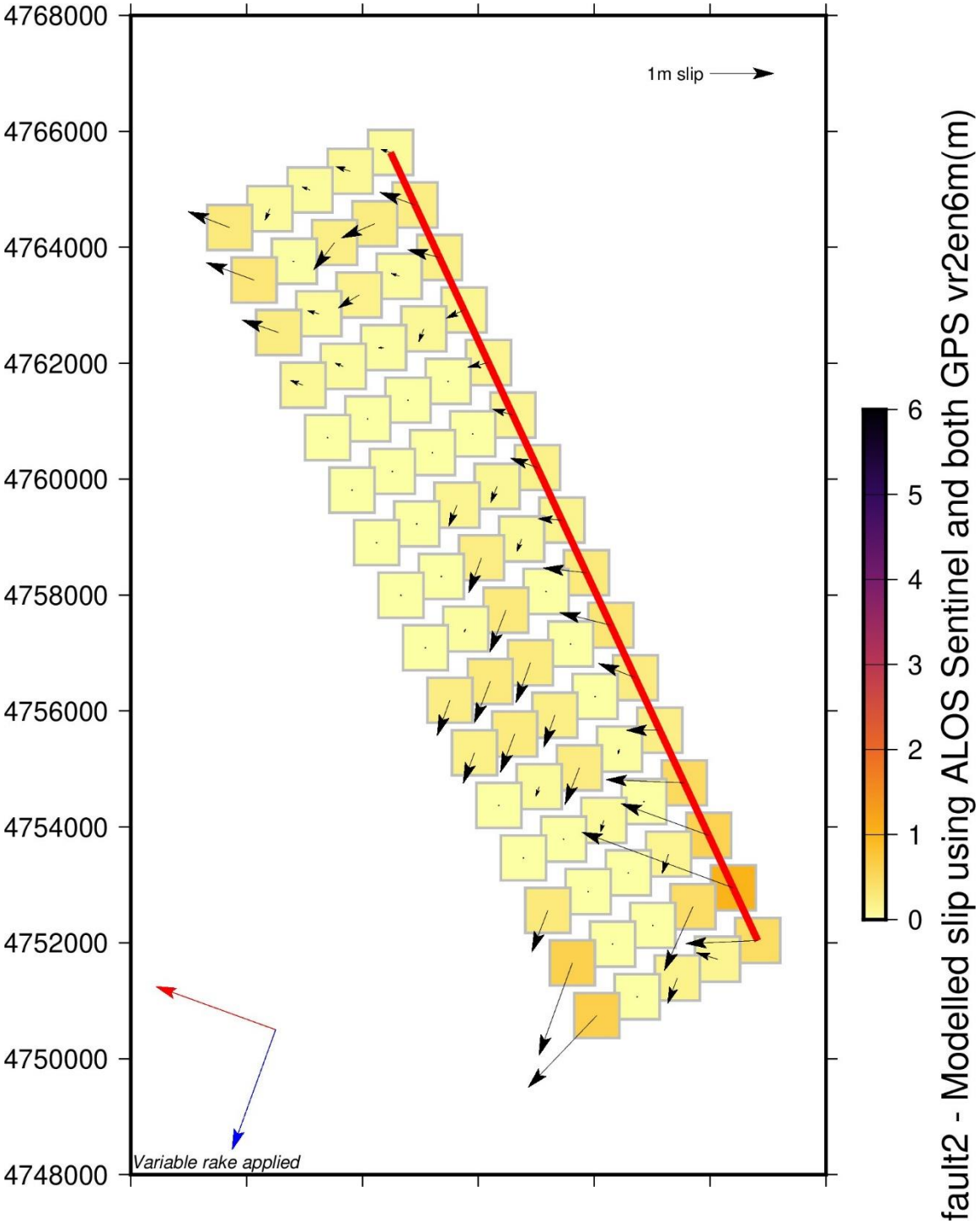

Fault 3 Monte Vettore N

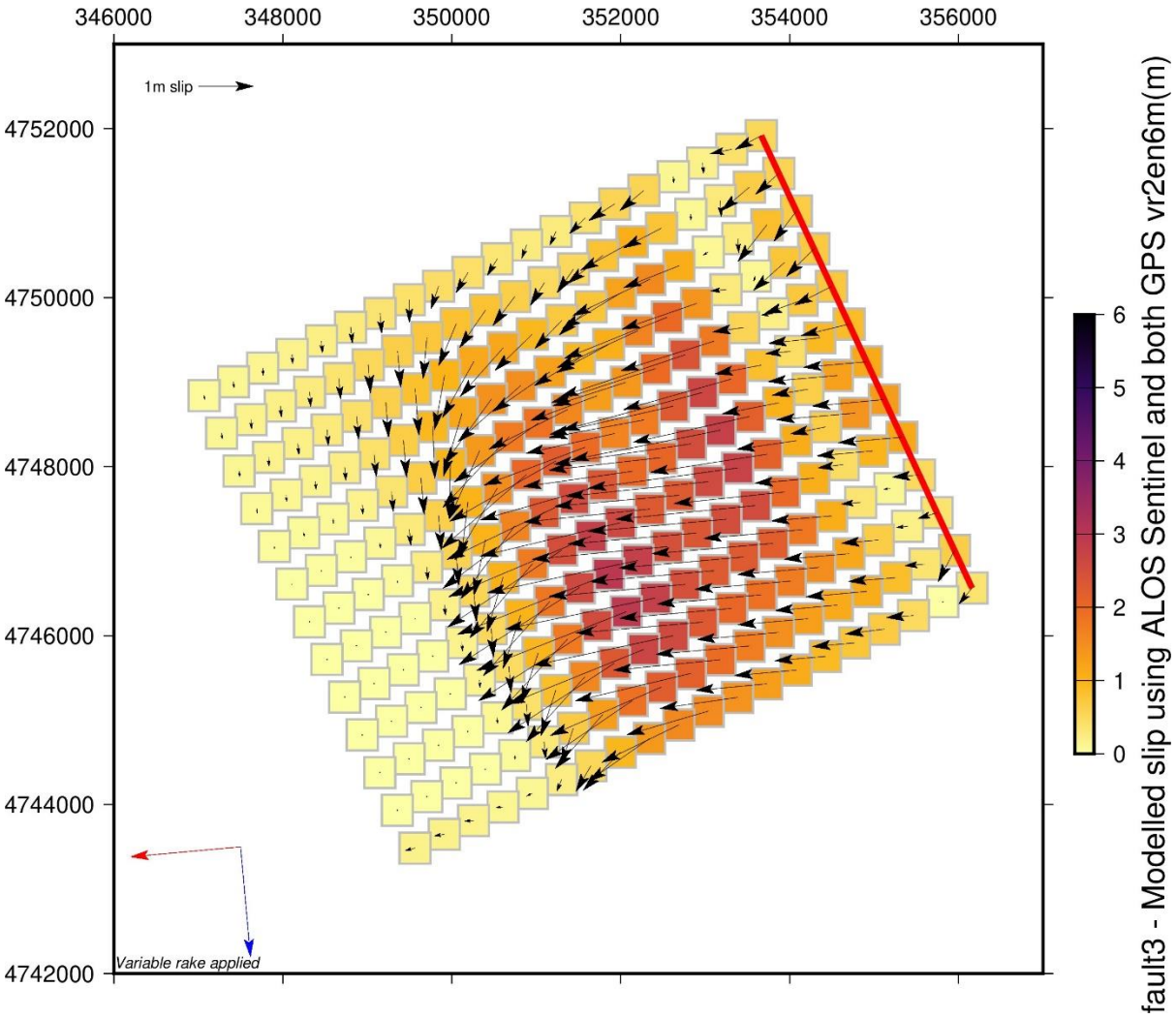

Fault 4 Monte Vettore central

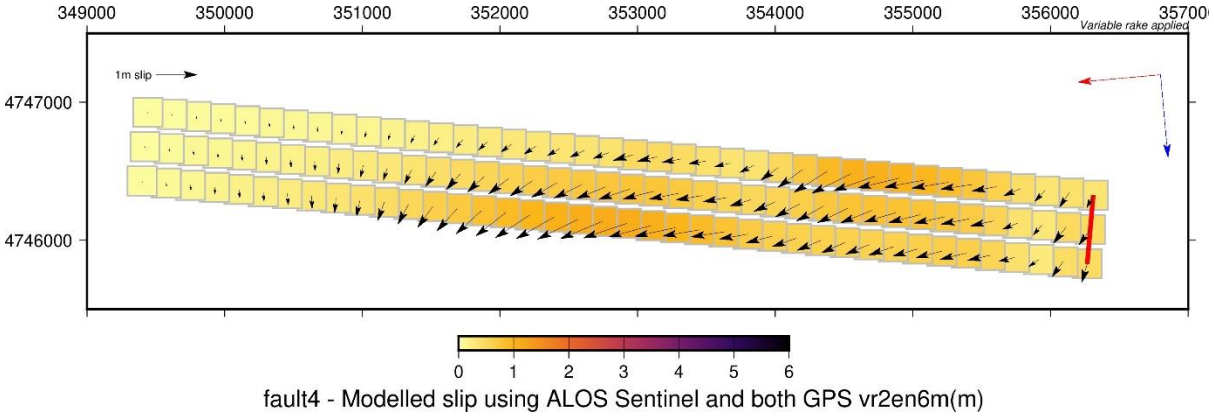

fault4 - Modelled slip using ALOS Sentinel and both GPS vr2en6m(m)

Fault 5 Monte Vettore central

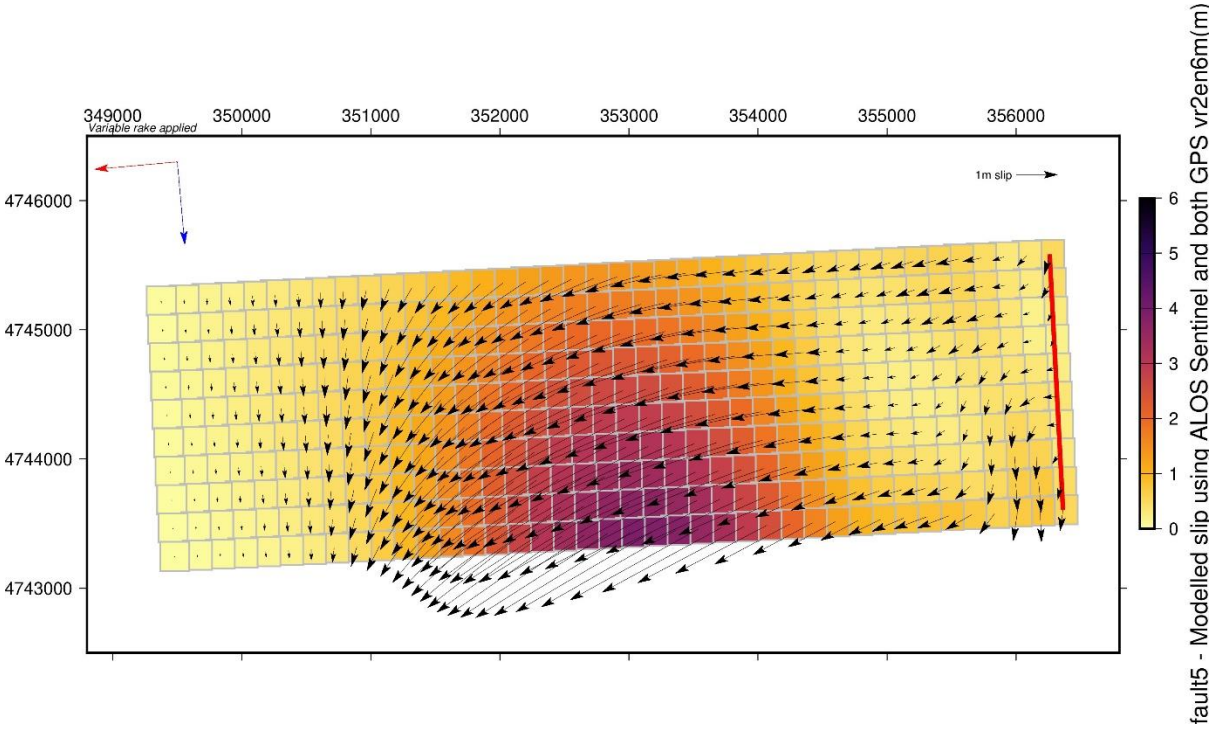

Fault 6 Monte Vettore central

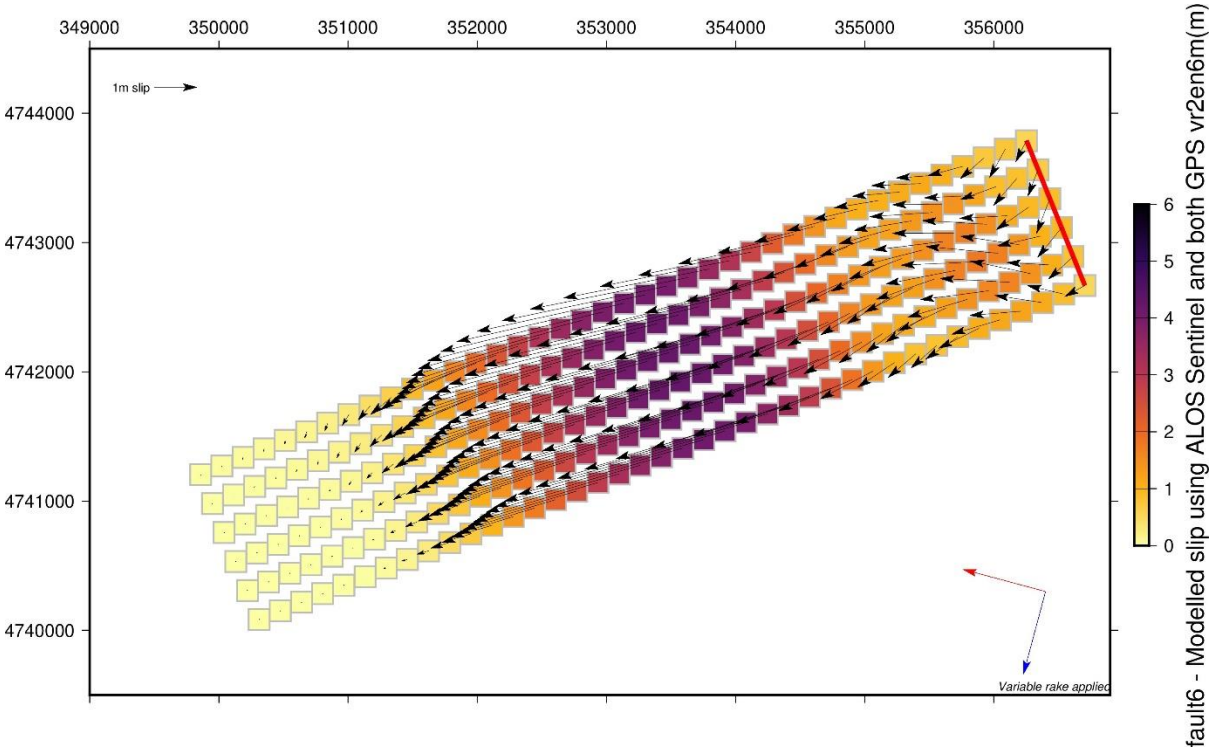

Fault 7 Monte Vettore central (incl Scoglio dell'Aquila)

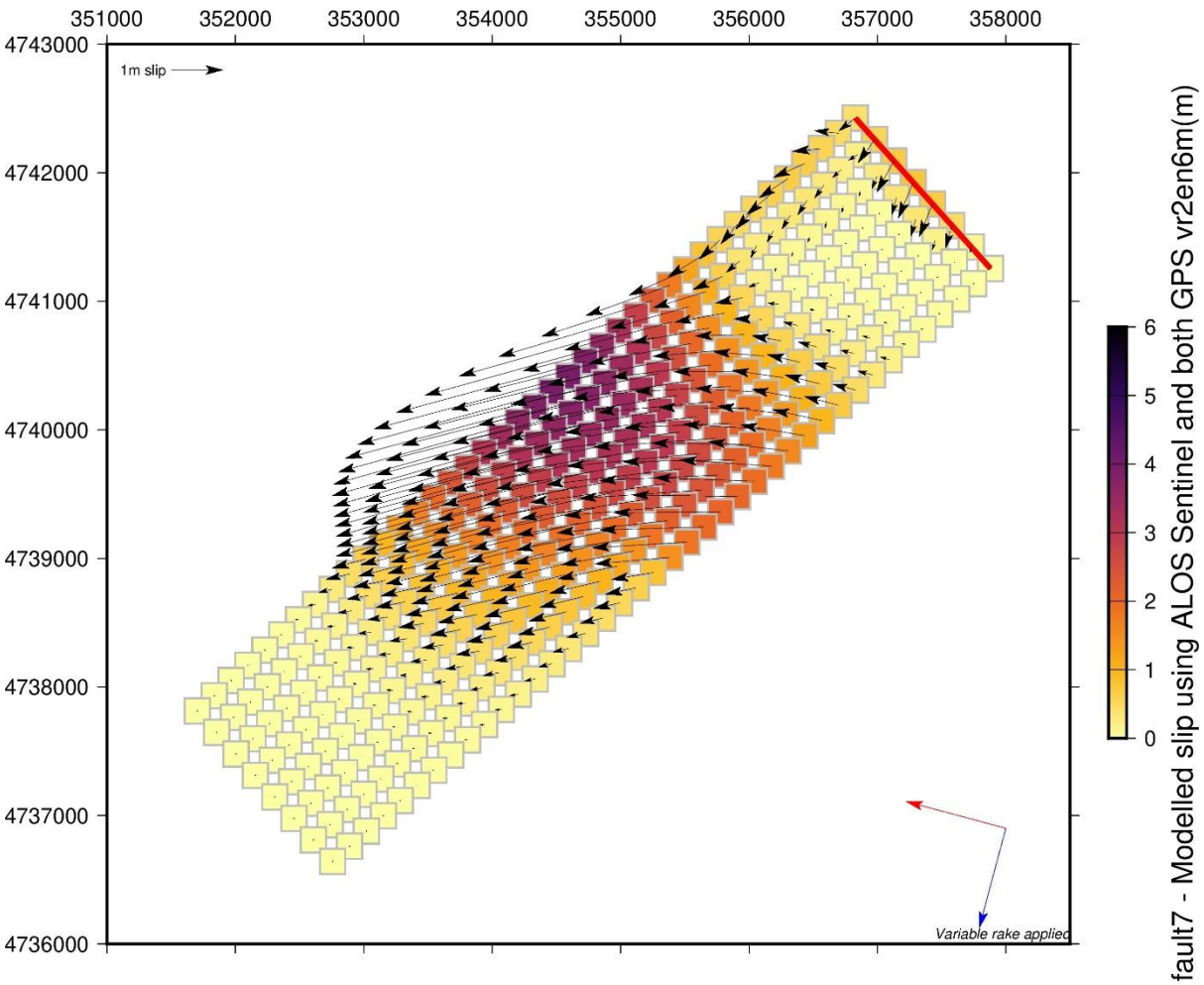

Fault 8 Monte Vettore S

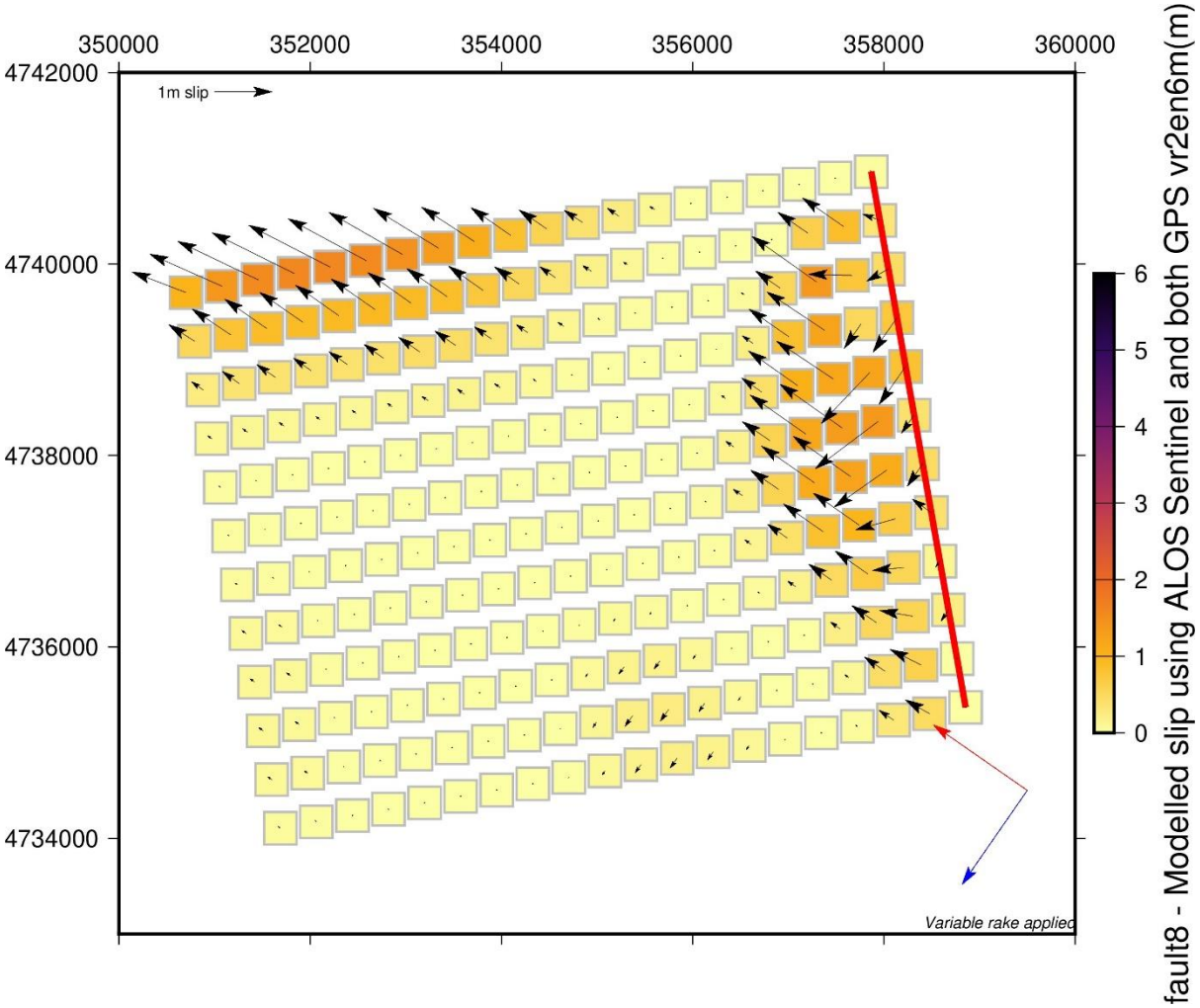

Fault 9 Minor Synthetic

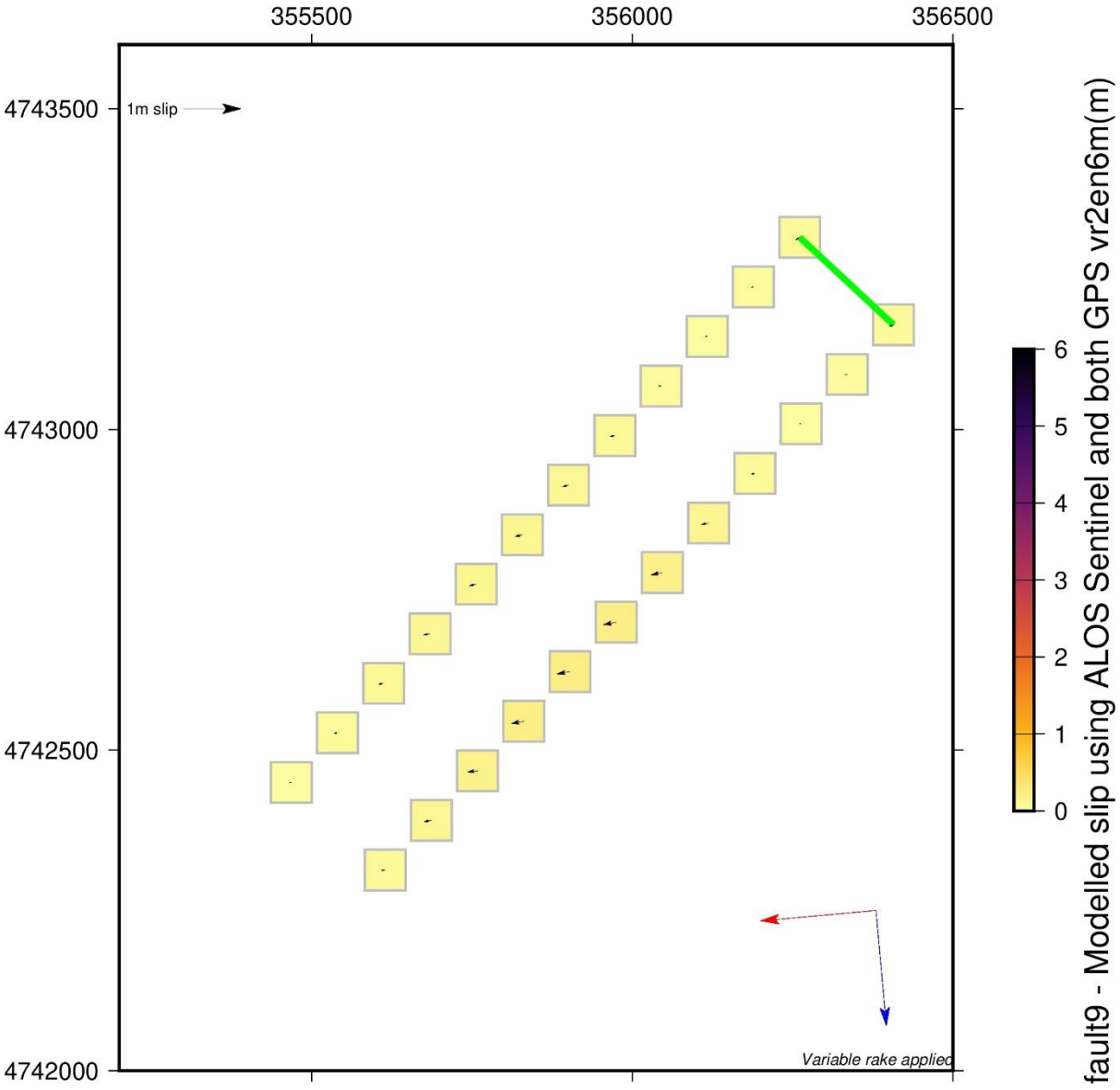

Fault 10 Minor Synthetic

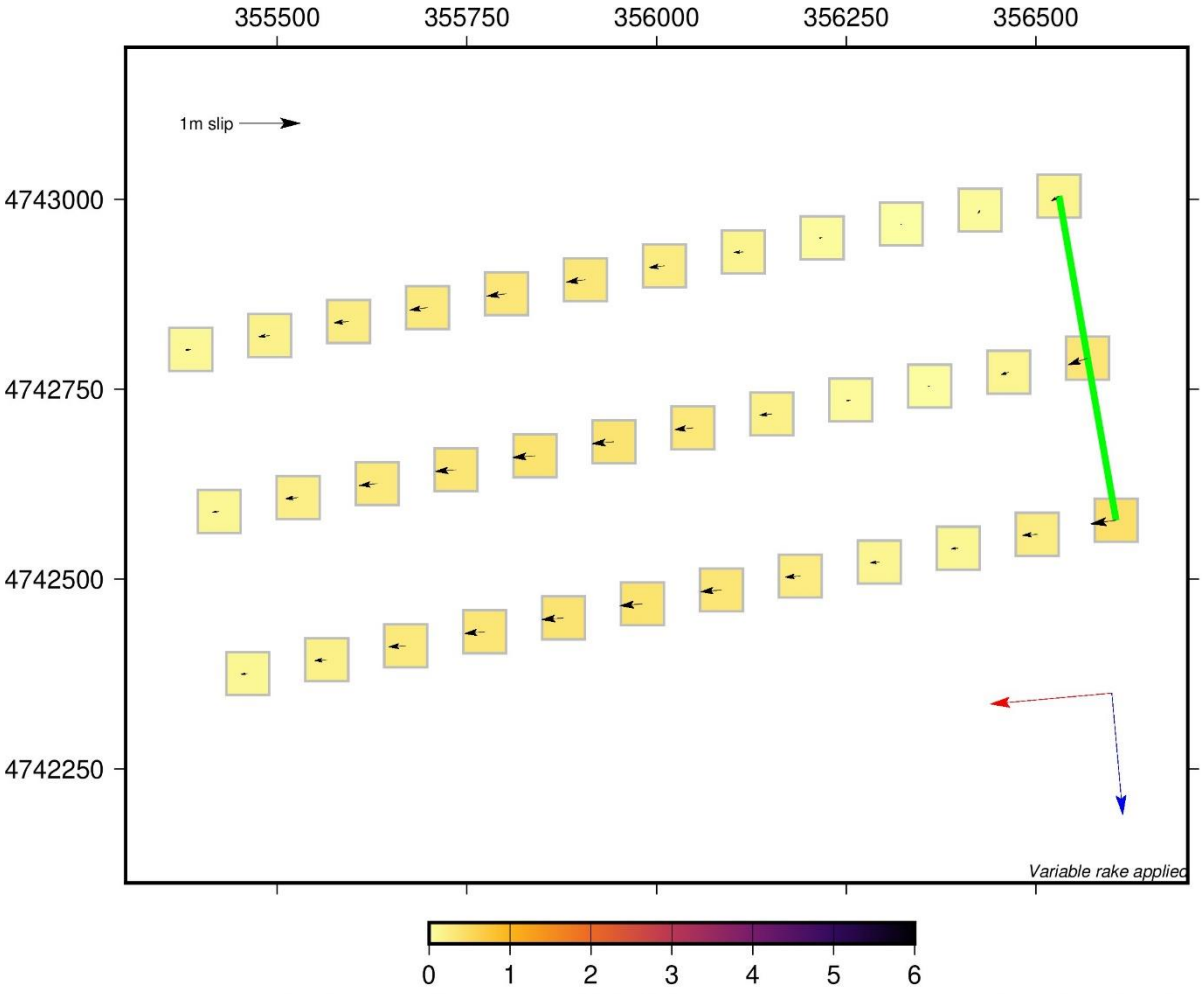

fault10 - Modelled slip using ALOS Sentinel and both GPS vr2en6m(m)

Fault 11 Minor Synthetic

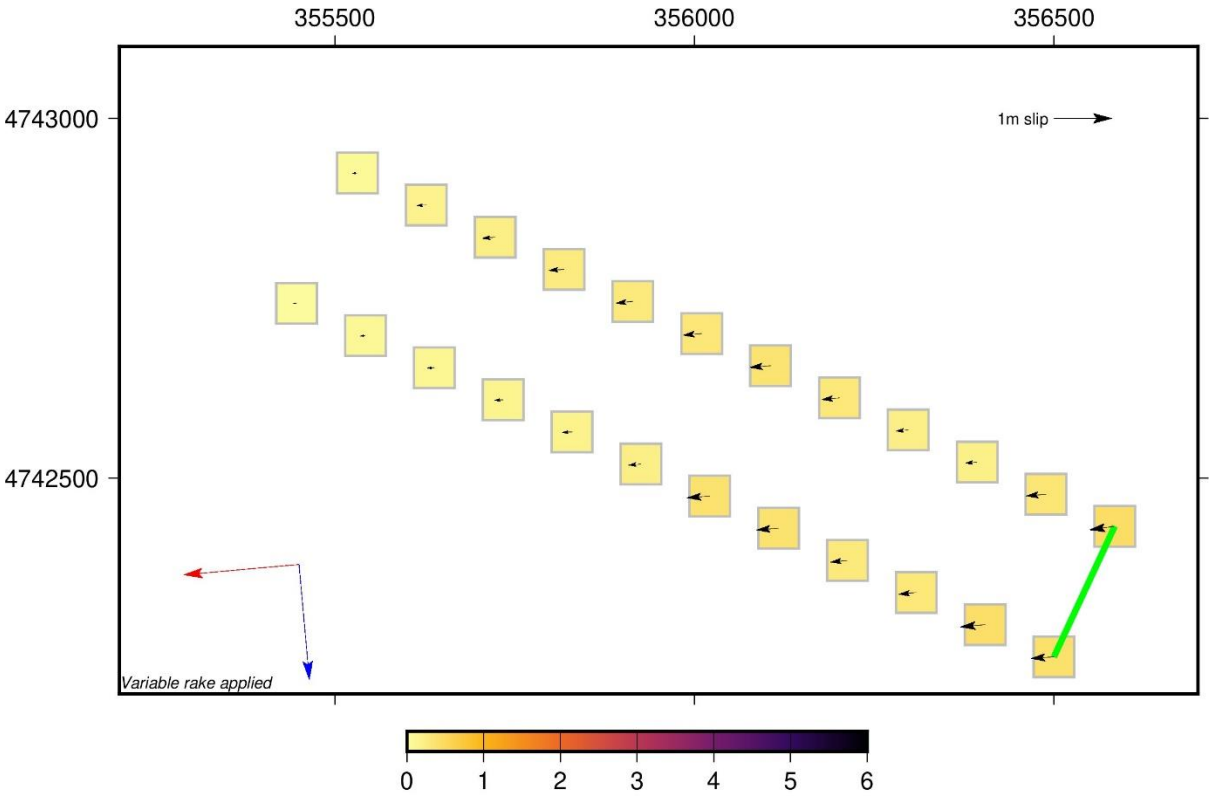

fault11 - Modelled slip using ALOS Sentinel and both GPS vr2en6m(m)

Fault 12 Synthetic

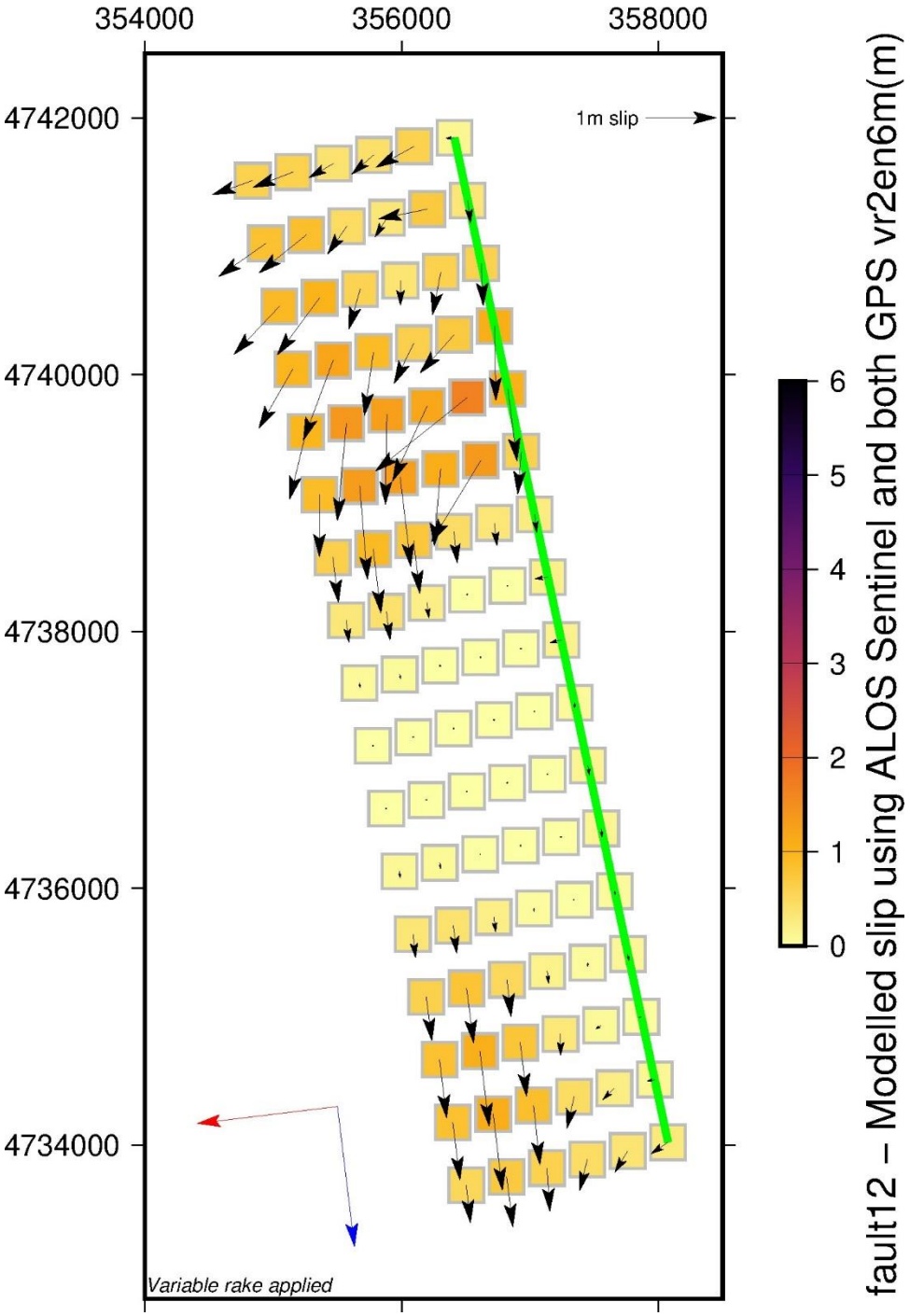

Fault 13 Antithetic

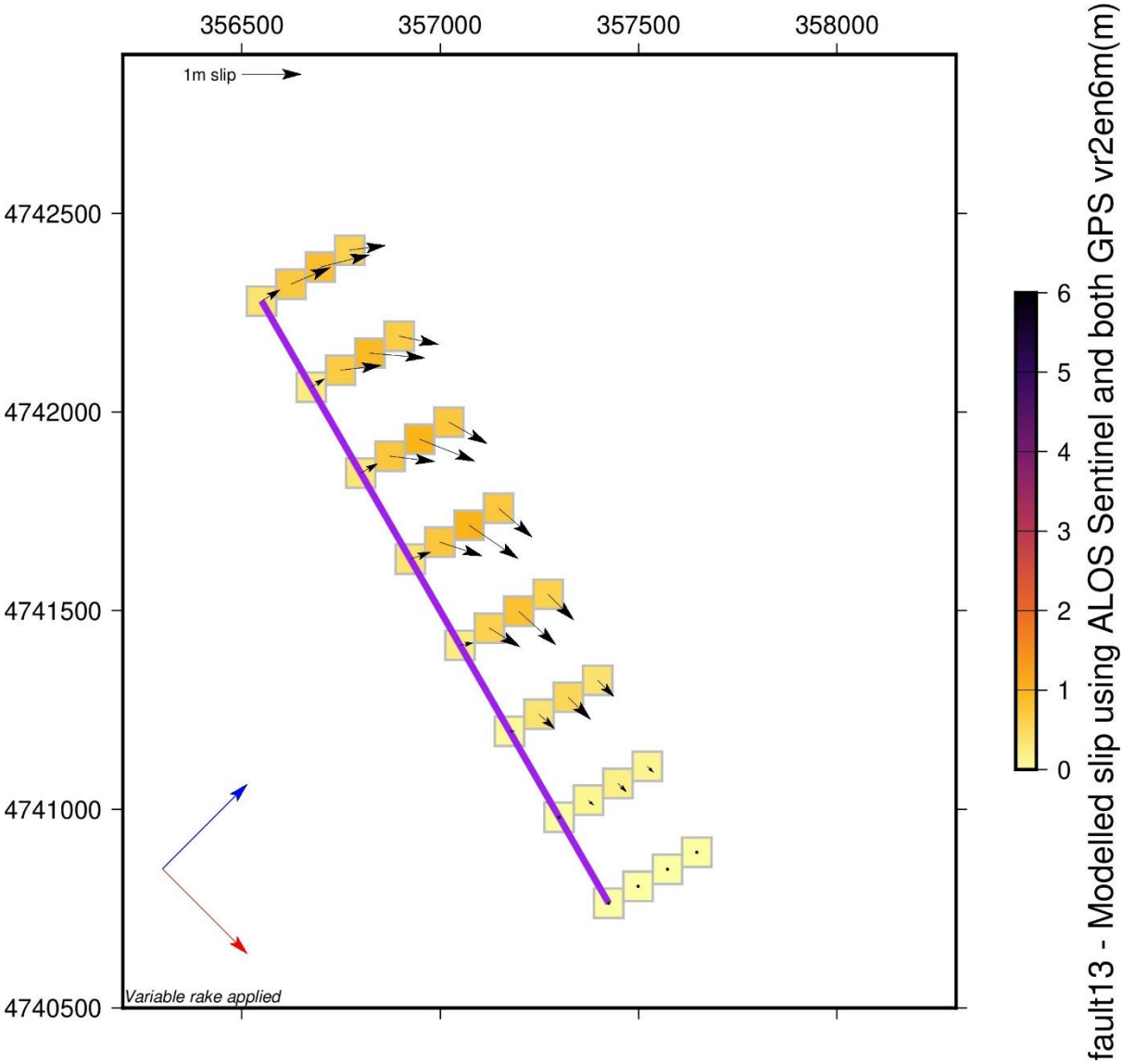

Fault 14 Minor Antithetic

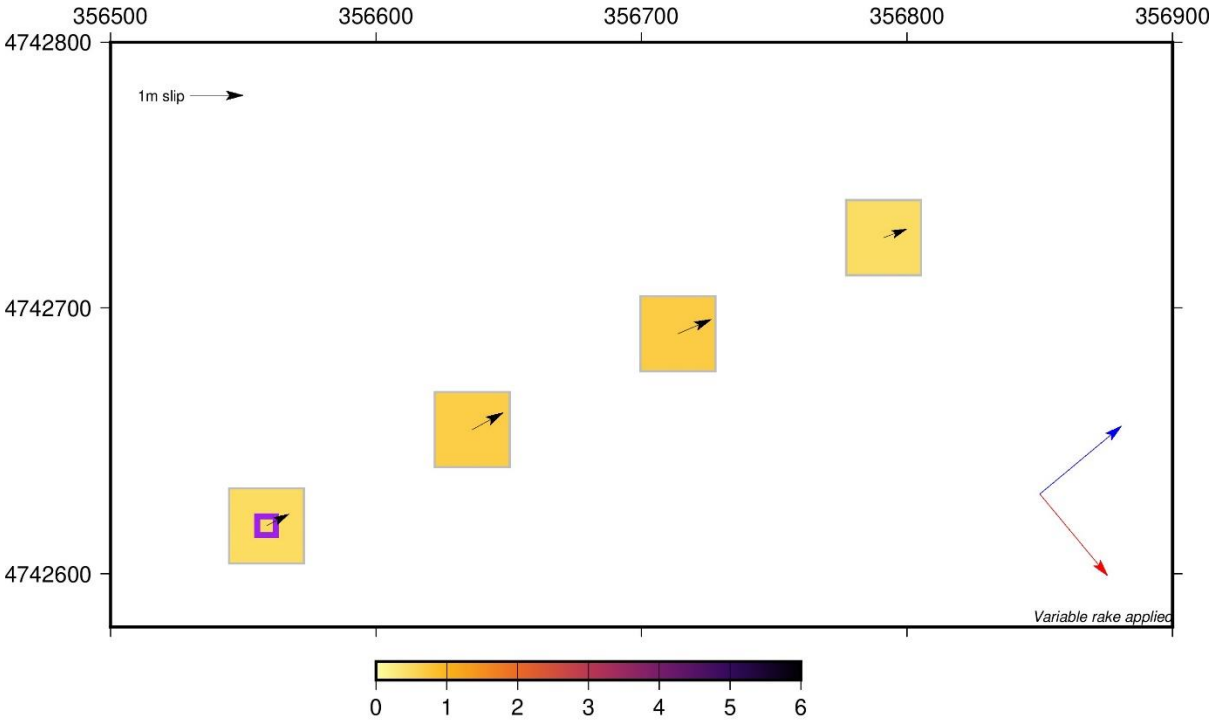

fault14 - Modelled slip using ALOS Sentinel and both GPS vr2en6m(m)

Fault 15 Antithetic

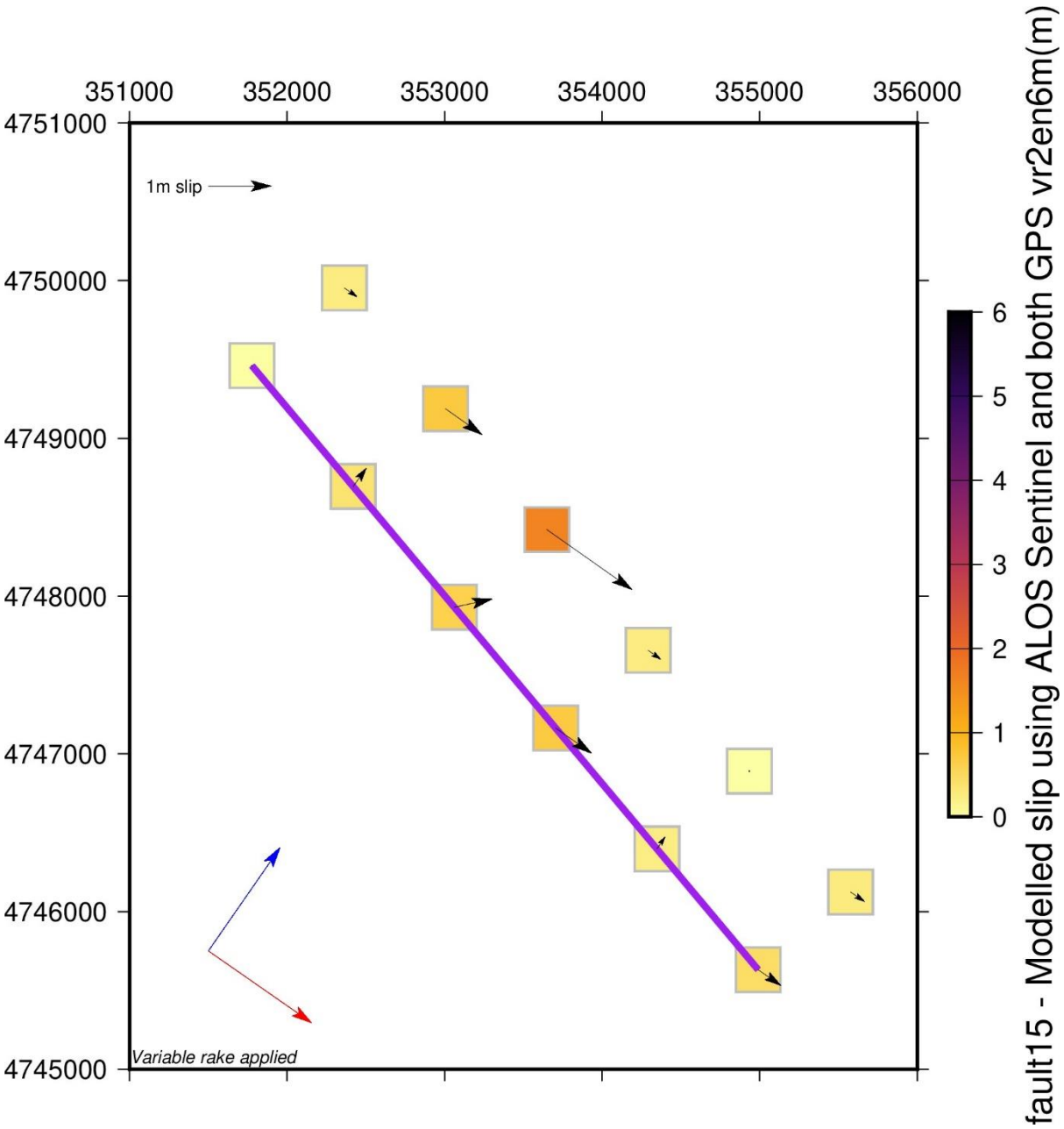

Fault 16 Norcia Antithetic

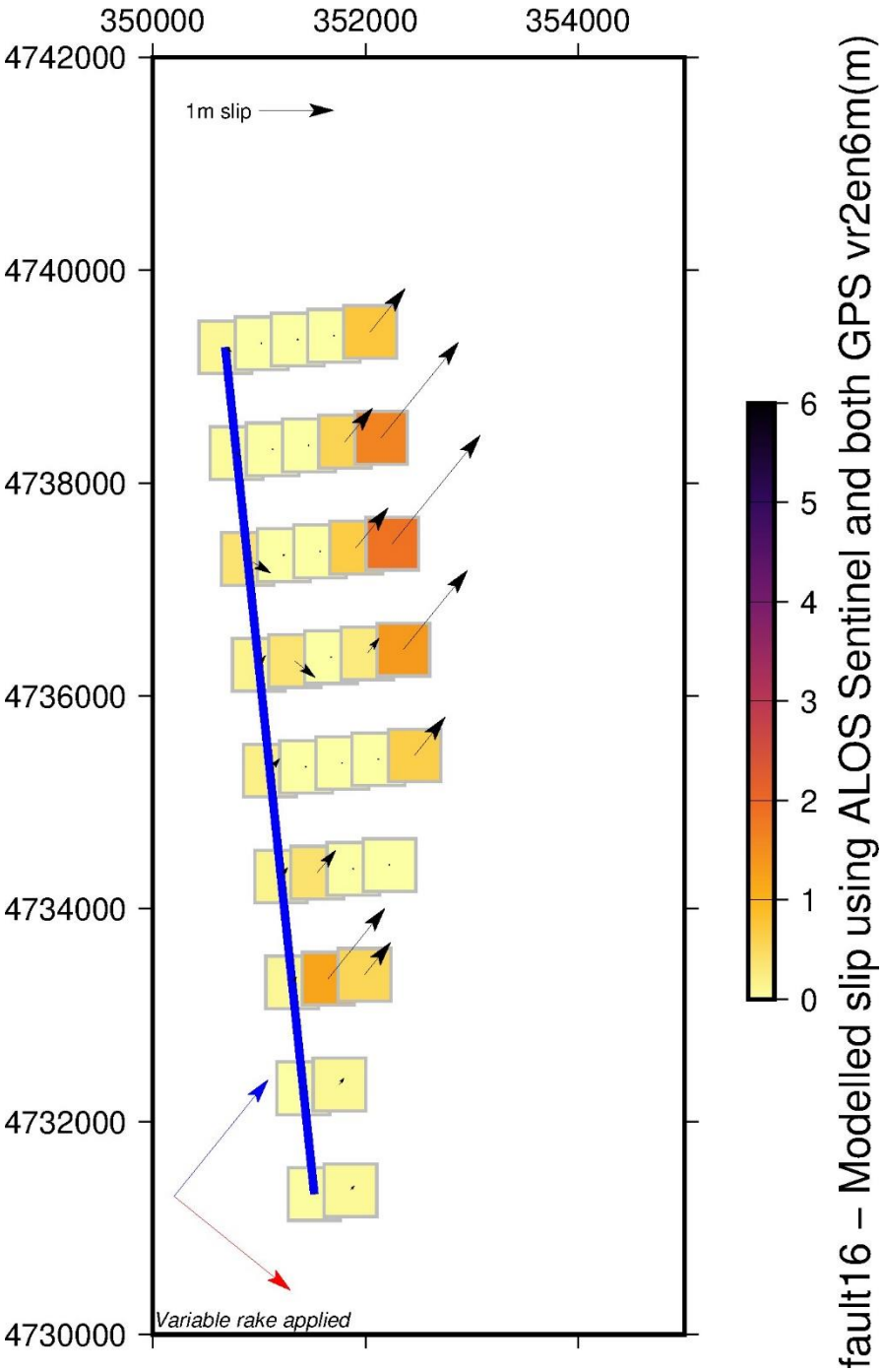

Fault 17 Pian Piccolo

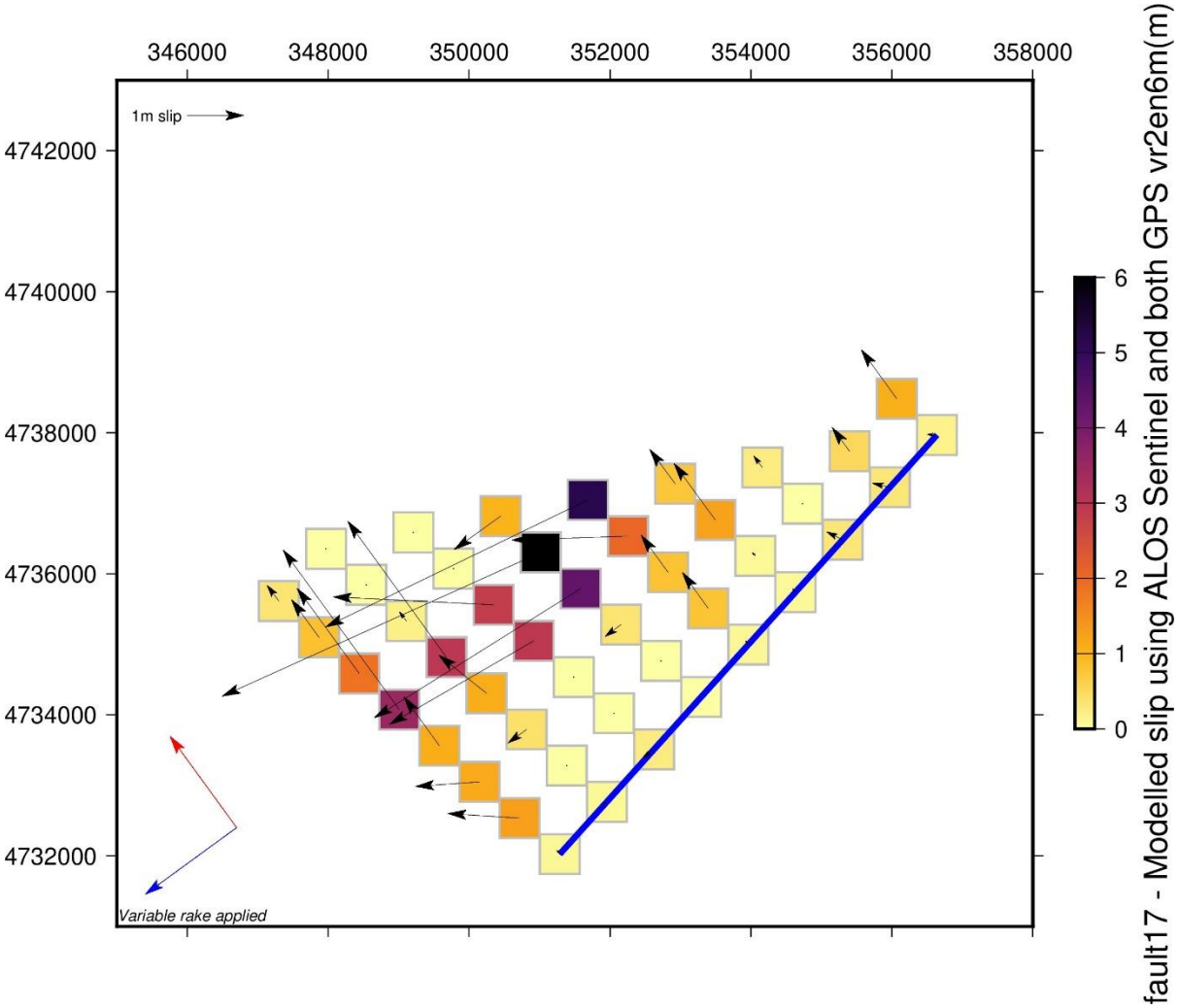

Fault 18 Laga

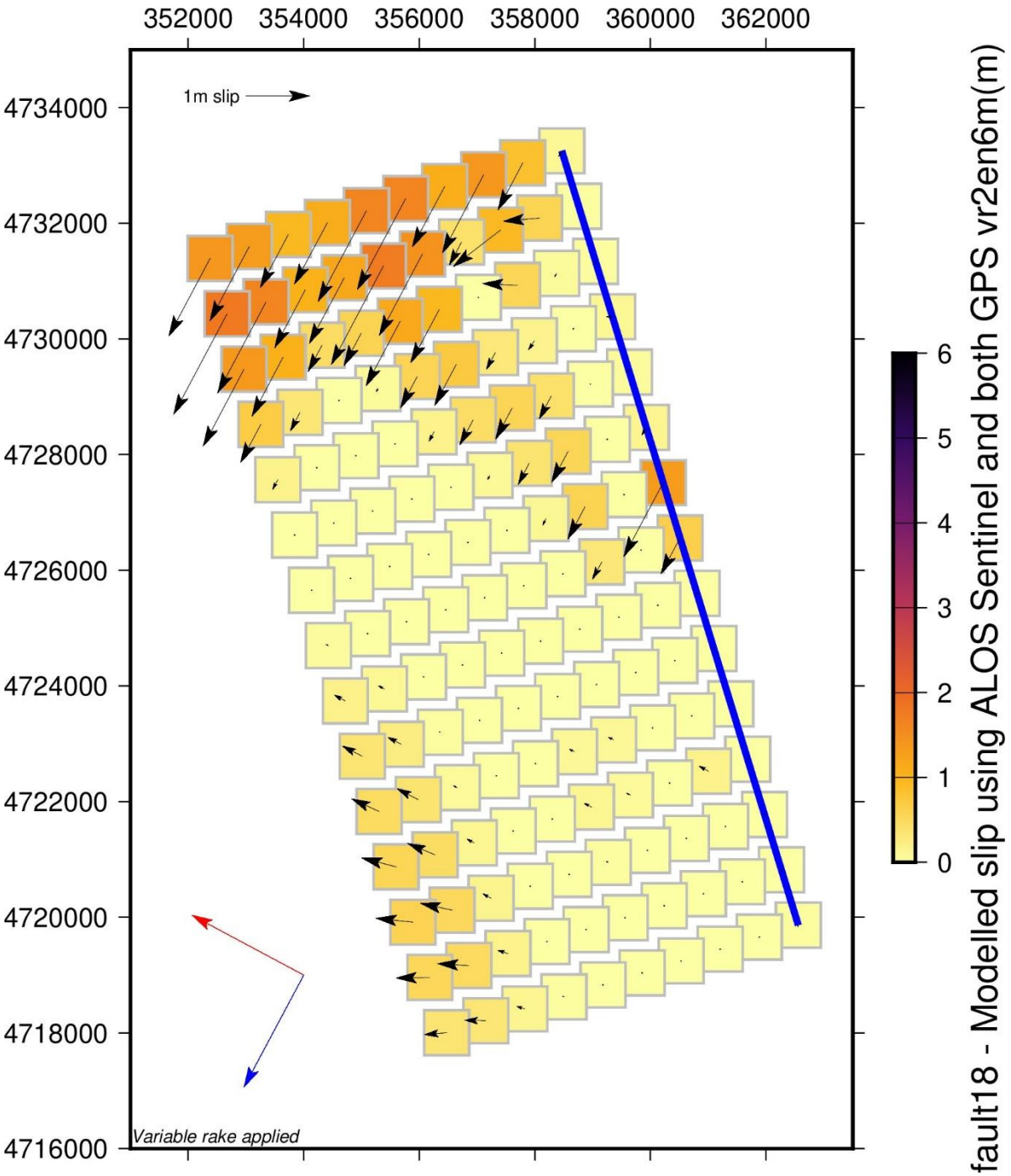

Fault 19 Monte Vettore spur

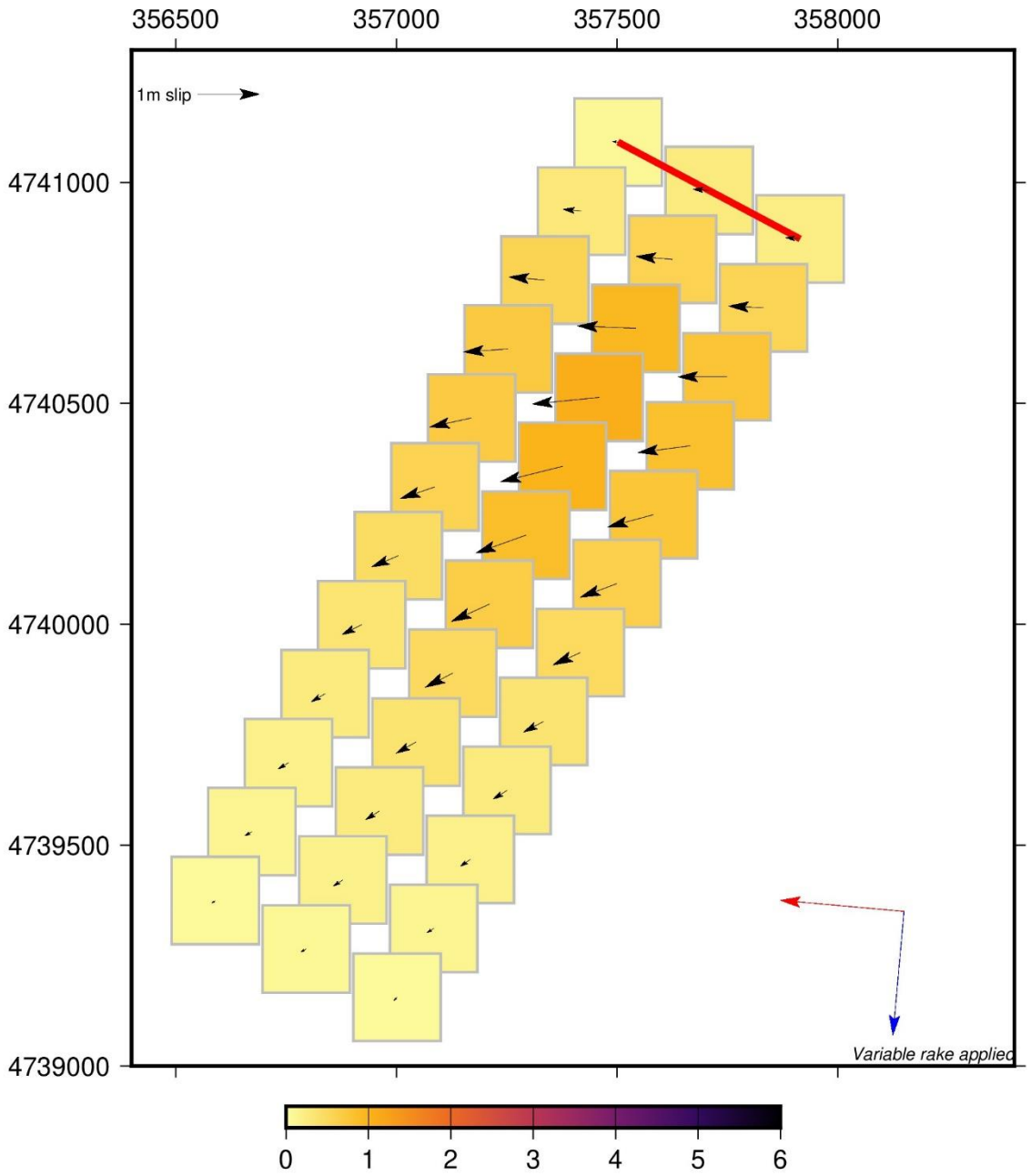

fault19 - Modelled slip using ALOS Sentinel and both GPS vr2en6m(m)

APPENDIX 3B

Comparison of my Pleiades results with those of Delorme et al., 2020

The results from the Pleiades data that I have used as the basis for my inverse modelling are shown in **Figure 3B1**. As noted in Chapter 3 of my thesis, I restricted the area used by (1) seeking to avoid areas of generally noisy data further N and S, (2) (to the W) avoiding areas with a long-wave sinusoidal artefact and (3) within the model itself (not shown in this figure) limiting data to within 1 km of the modelled fault traces.

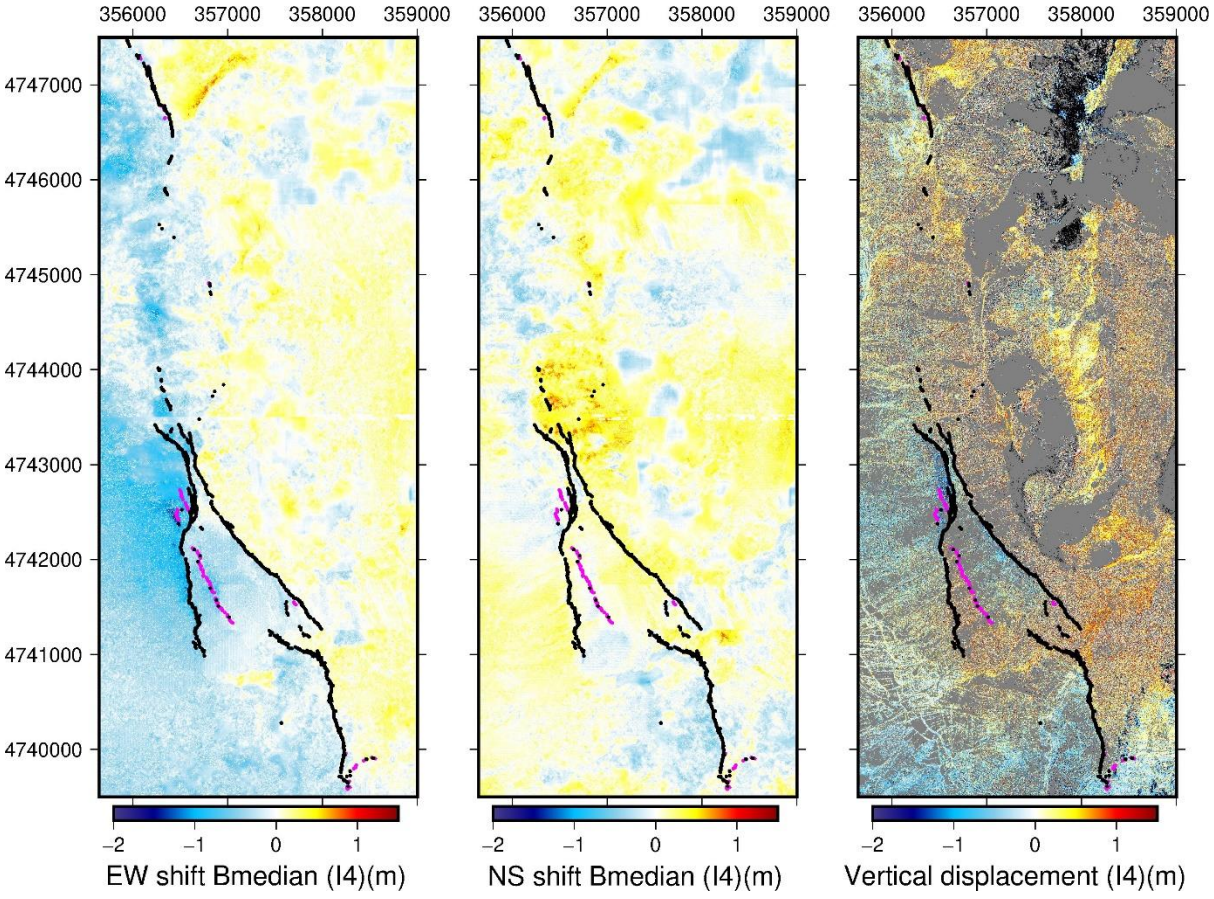

Figure 3B1 Displacements from filtered results of correlation tool (EW, LH panel, NS centre panel), and vertical differencing (RH panel)

3B (a) Comparison of displacement results

Delorme et al., 2020, the only previous study to have used Pleiades optical satellite data as one of a number of datasets in inverse modelling of the Norcia earthquake, initially resolved both horizontal and vertical co-seismic displacements using the full extent of the overlap between the Pleiades datasets. Although they do not use the full extent of the data in their

inversion, I have visually compared their wider-scale results with my own for the extent of the area for which I applied the COSI-Corr correlation tool (56 km^2) (which includes the area with the long-wave sinusoidal artefact). The visual comparisons are shown at **Figures 3B2 to 3B4**.

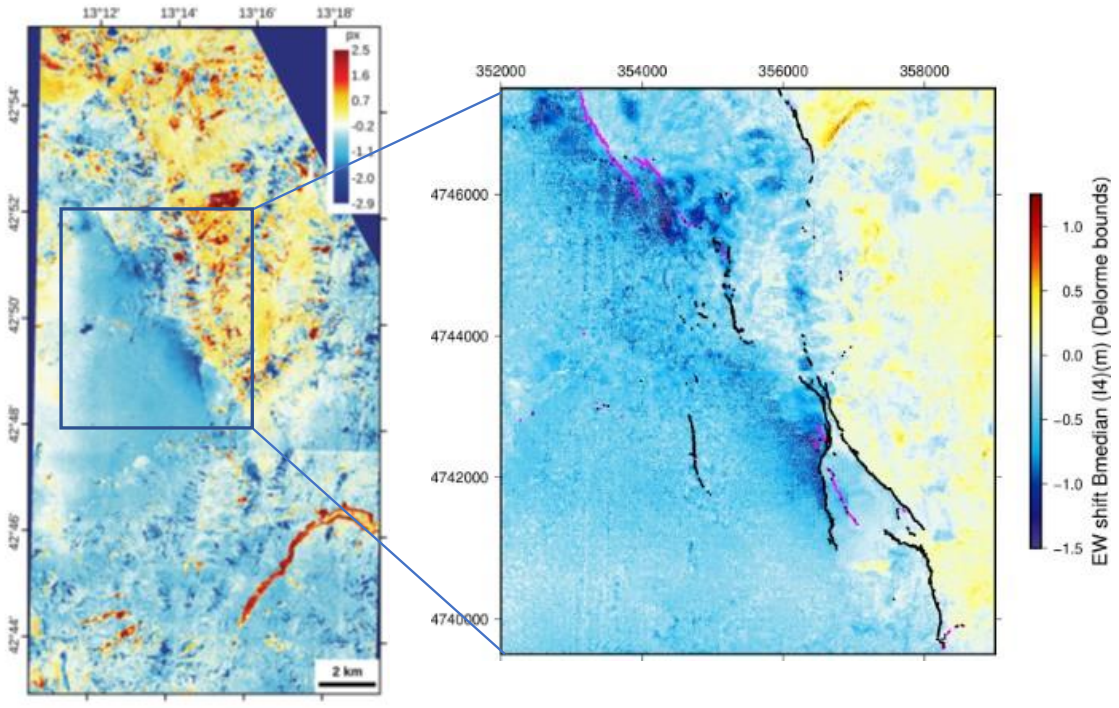

Figure 3B2 Comparison of Delorme et al, 2020 EW displacement (from their Figure S1) (LH panel) with my EW displacement values for the area shown (RH panel), using the same colour palette as far as possible.

I have made the comparisons using (so far as possible) the same colour palettes as in the Delorme et al. study. In that study, the colour palettes differ between their figures and are expressed in pixels (each 50 cms x 50 cms). My comparisons may therefore not be entirely accurate in every case. However, the results (**Figure 3B2**) suggest that the noise in the EW displacement field is significantly reduced in my results, particularly in the footwall, with values much reduced from the up to > 1m E displacement seen in the Delorme et al. results.

In the NS displacement field (**Figure 3B3**) my results are noisier than my EW results, but still markedly less so than the Delorme et al. results, which show N movement in both hanging wall and footwall with very patchy results for the footwall with a mixture of N movement of

up to ~1 m and S movement of ~0.4 m (note that Delorme et al.'s colour palette has white at ~20 cm N movement, rather than zero).

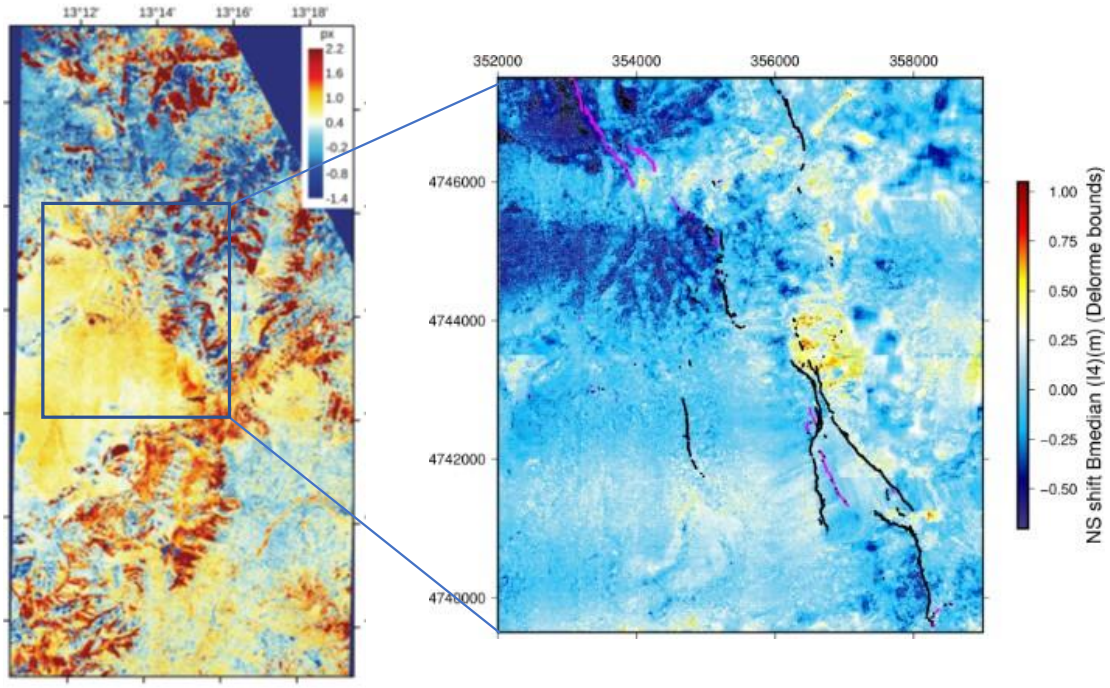

Figure 3B1 Comparison of Delorme et al., 2020 NS displacement (from their Figure S1) (LH panel) with my NS displacement values for the area shown (RH panel), using the same colour palette so far as possible.

My NS (and vertical) results show a sinusoidal effect to the W of a line at ~355600 33T UTM, which seems to be absent from Delorme et al.'s NS results. However, Delorme et al. refer to removal of a long wavelength fault-perpendicular signal from both the NS and vertical results by extracting stacked profiles from an area with no significant tectonic deformation to fit a long wavelength spline function. If this is the same signal, this adjustment may explain the difference.

The vertical displacement fields (**Figure 3B4**) are more difficult to compare visually at this scale due to the difference in data coverage (it is unclear to me how Delorme et al. have smoothed their results to achieve their overall coverage in this figure).

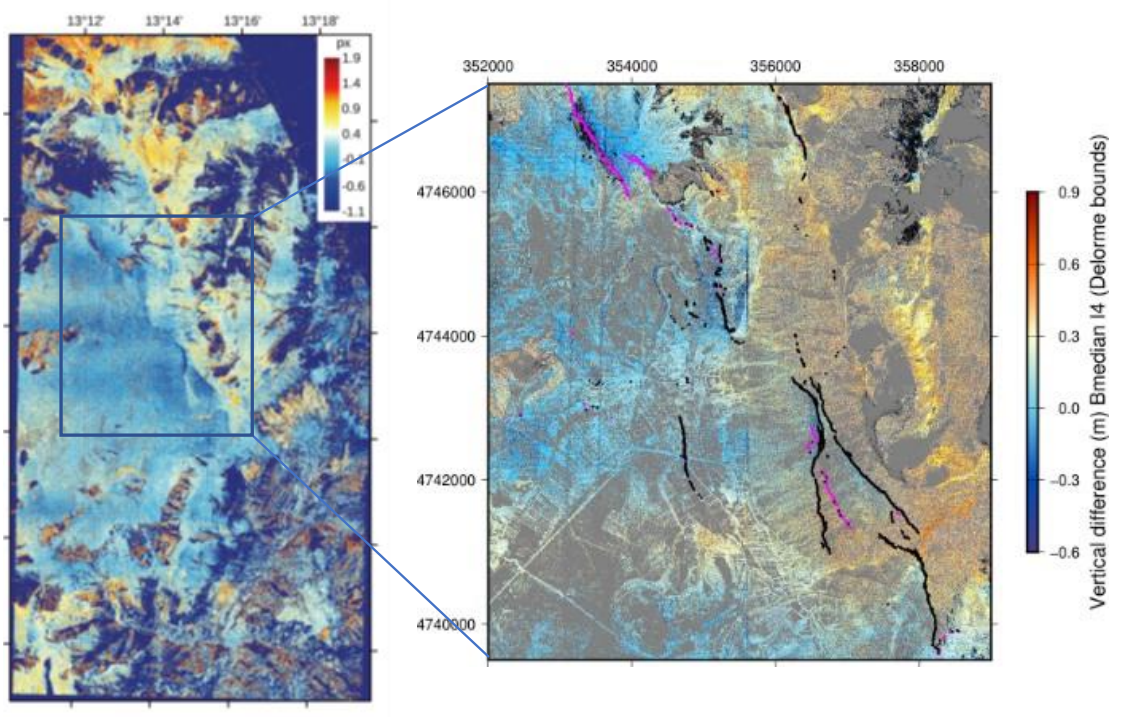

Figure 3B4 Comparison of Delorme et al. (2020) vertical displacement (from their Figure S1) (LH panel) with my vertical EW displacement values for the area shown (RH panel), using so far as possible the same colour palette.

Note again that white in the colour palette is not at zero – here it is at ~25 cm upwards displacement. In this case, both sets of results show a sinusoidal effect to the W of ~355600 33T UTM, which presumably remains in the Delorme et al. results despite their removal of a fault-perpendicular long wavelength signal. In the footwall, areas which show no data in our results are shown as having > 50 cm of downward movement in Delorme et al.'s results.

3B (b) Other possible artefacts in the results

At smaller scale Delorme et al. refer to a second residual signal in the along-track direction, which they say is related to CCD misalignments and satellite jitter artefacts and to topographic artefacts which correspond to the drainage network. Their vertical displacement results at this smaller scale are shown in their Figure 2. This area overlaps with the restricted area I have used for the Pleiades data in my inversion, where I have excluded the area with the sinusoidal effect. In **Figure 3B5** panel (a) shows the extent of overlap with the Pleiades data I have used (red dashed box). My vertical deformation results for that overlapping area are shown in panel (b) in the figure. Delorme et al.'s results for the area

that they used for their shallow surface modelling are shown in panel (c). Delorme et al.'s colour palette has again been used in (b) for the purposes of the comparison (note that white is again not zero, but in this case ~20 cm upwards displacement).

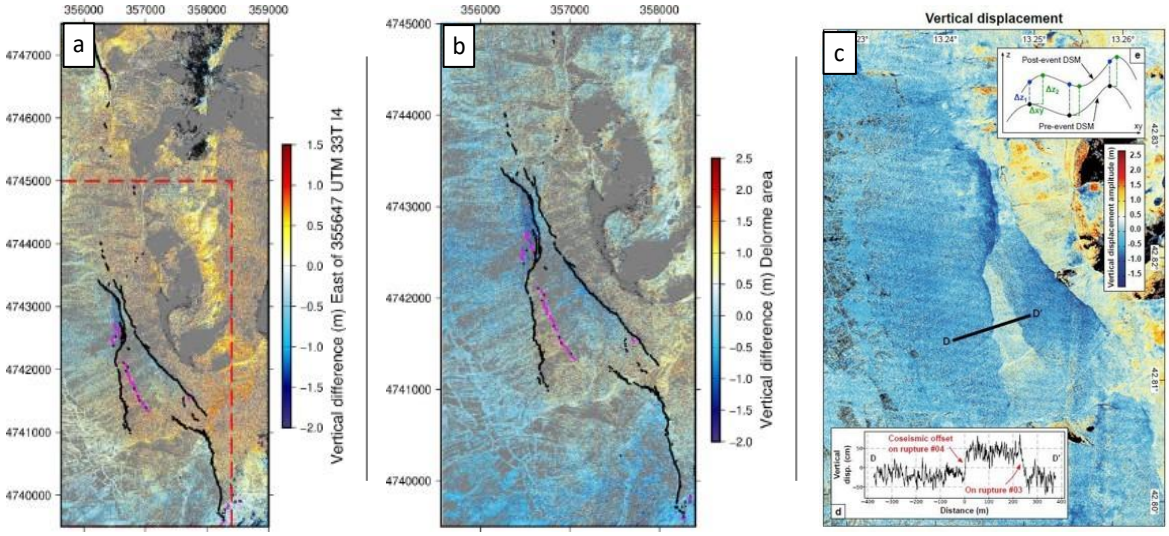

Figure 3B2 Comparison of (c) Delorme et al., 2020 detailed vertical displacement (from their Figure 2) with (b) my vertical displacement values for the area shown, using so far as possible the same colour palette. (a) shows the overlap between the detailed area shown in (c) and the area I have used for my inversion (red dashed box) relative to the area. The far-left hand area used by Delorme et al. has been omitted from the comparison with my results (b) as it was not used for my modelling because of the sinusoidal effect seen W of Easting 355647 UTM 33T.

I investigated the apparent along-track signal artefacts seen in Delorme et al.'s Figure 2 and the residual topographic signals identified at much smaller scale in their Figure S2 to see whether similar signals appeared in my data. The first feature I inspected was the ENE-WSW trending sub-parallel lines in Delorme et al.'s figure. I concluded that, although similar features were apparent prior to application of my filtered offset, they coincide with topographical features, in particular the ENE-WSW trending gullies in the W slope of Monte Vettore (as Delorme et al. have also suggested). If the images are misaligned, the differencing process introduces the artefacts by comparing pixels external to the gulley with pixels within the gulley. Once my offsets were applied, this signal disappeared in all of the displacement fields. In my results (**Figure 3B5** (b)) although the gullies apparently show up,

they are areas of higher data density (rather than areas of relative vertical displacement) and therefore appear more prominent. Therefore, I do not consider them to be artefacts in my results.

Delorme et al.'s figure S2 also shows regular spatial aliasing with an amplitude of ~ 6-8 cm, in a fault-perpendicular direction in one of the images (showing E-W displacement). The vertical displacement results shown in **Figure 3B5** (c) also suggest a similar, regular signal in a NNE-SSW direction. I have not been able to identify signals similar to either of these in any of my displacement fields.

3B (c) Noise in the data

As to the vertical displacements shown, Delorme et al.'s figure shown in panel (c) in **Figure 3B5** (zoomed-in relative to their Figure S1) illustrates more clearly the noisy results in the footwall (albeit that some of this detail is hidden behind the scale bar and other sub-figures in the figure), including areas immediately adjacent to the main Monte Vettore fault.

In their joint inversion of GPS, InSAR and Pleiades data, Delorme et al. down-sample their 3-dimensional displacement results from the Pleiades data to either a resolution of 250 m (according to the caption to their figure 5) or 0.5 km (accompanying text). They also limit their use of the data to results within 1 km of the trace of the co-seismic surface ruptures, to "fill the measurement gap in the ALOS-2 data set". The data they used is shown in **Figure 3B6**.

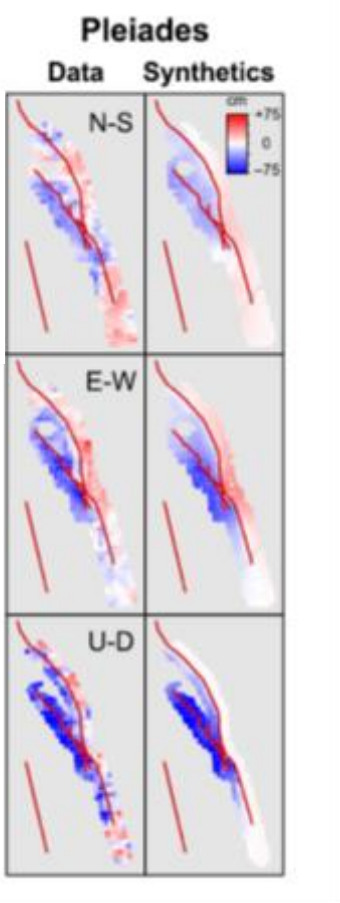

Figure 3B3 Delorme et al., 2020 modelled observed 3-dimensional displacement from Pleiades (Data), and synthetic displacements predicted by the best model deduced from the joint inversion of GPS, InSAR, and Pleiades data (Synthetics)

Even at this scale, it is possible to identify data within the hanging wall in particular arising from the anomalous results identified above in the horizontal displacements that are within 1 km of the main ruptures, and similar anomalies in the vertical displacement data. I note that the N-S displacements appear to have undergone a shift from the values towards the S compared to the results in their Figure S1 (see **Figure 3B3**).

3B (d) Summary

Given that the Delorme et al.'s Pleiades input data to their inversion (1) are noisy, (2) include data from an area that I (and Delorme et al.'s figure S1) have identified as being subject to a long-wave sinusoidal distortion, and (3) suffer from uncorrected topographic and regular spatial aliasing artefacts, the reliability of the Pleiades data set within Delorme et al.'s inversion must be open to question. Whilst more limited in area, my Pleiades data

results appear to be more robust as a result of my approach to differencing the datasets, filtering to reduce noise and omitting the more questionable areas of data outside the main areas of co-seismic displacement. They therefore provide a potentially more reliable source of detailed near-fault data for the joint inversion.

APPENDIX 4

Part 4.1 Meterff Results

Table of fault geometry used for joint inversion using 2 fault segments

Strike	Dip	Rake	Easting/1000	Northing/1000	Length (km)	Surface	Depth (km)	Patches1	Patches2	ID
167.6	70	-60	355.305	4744.153	0.047	0	0.5	5	50	1
142.1	65	-79	355.336	4744.096	0.086	0	0.5	9	50	1
167.6	70	-150	355.305	4744.153	0.047	0	0.5	5	50	2
142.1	65	-169	355.336	4744.096	0.086	0	0.5	9	50	2

Table of fault geometry used for joint inversion using 3 fault segments

Strike	Dip	Rake	Easting/1000	Northing/1000	Length (km)	Surface	Depth (km)	Patches1	Patches2	ID
167.6	70	-60	355.305	4744.153	0.047	0	0.25	5	25	1
142.1	65	-79	355.336	4744.096	0.086	0	0.25	9	25	1
167.6	70	-150	355.305	4744.153	0.047	0	0.25	5	25	2
142.1	65	-169	355.336	4744.096	0.086	0	0.25	9	25	2
134	60	-65	355.34	4744.125	0.1	0	0.6	9	60	3
134	60	-155	355.34	4744.125	0.1	0	0.6	9	60	4

Appendix 4

Meterff Internal consistency checks

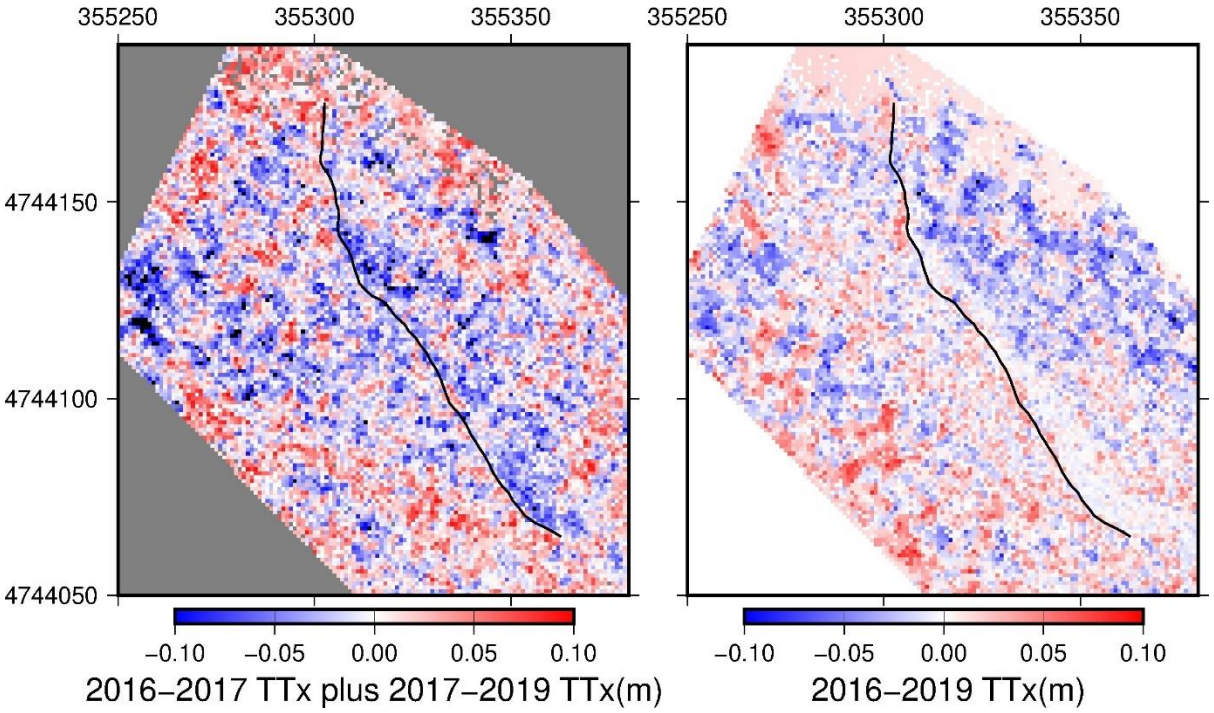

Figure 4.1 EW displacement results from the 2016-2017 pairing added to the results from the 2017-2019 pairing (LH panel), set against the EW displacement results from 2016-2019 pairing (RH panel).

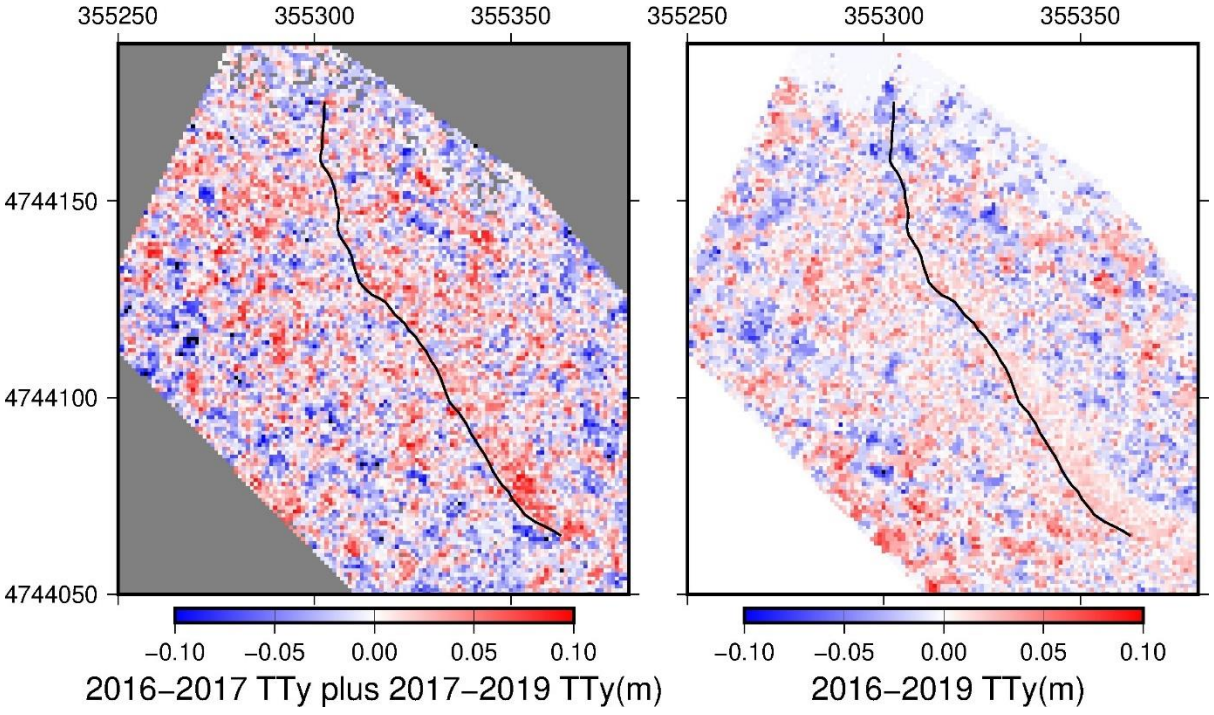

Figure 4.2 NS displacement results from the 2016-2017 pairing plus the results from the 2017-2019 pairing (LH panel), set against the NS displacement results from 2016-2019 pairing (RH panel).

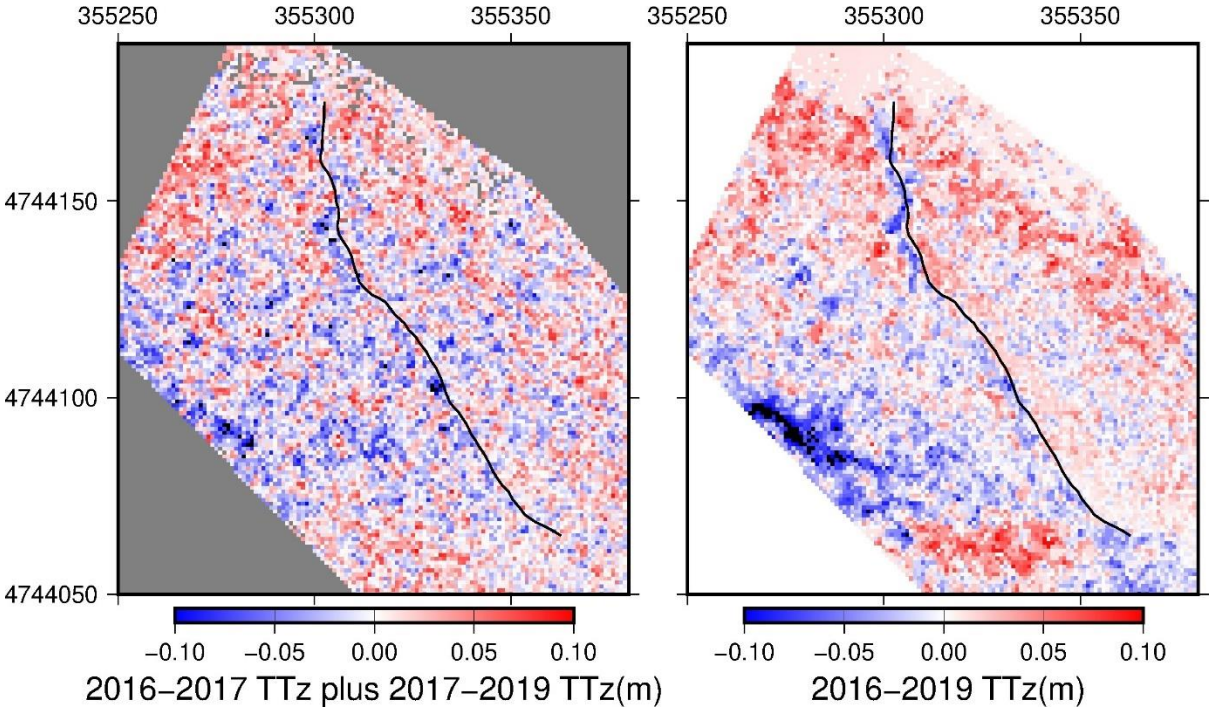

Figure 4.3 Vertical displacement results from the 2016-2017 pairing plus the results from the 2017-2019 pairing (LH panel), set against the vertical displacement results from 2016-2019 pairing (RH panel).

Meterff observed, model and residuals, using 2 fault segment geometry for 2016-2017, 3 fault segment for 2016-2019 and 2017-2019

In each figure, the magenta box in the observed (LH) panel is the area used to calculate the standard deviation values of the input data. Blue lines are modelled faults at surface, dashed green lines secondary structure in Meterff's footwall, red lines Meterff scarp.

2016-2017

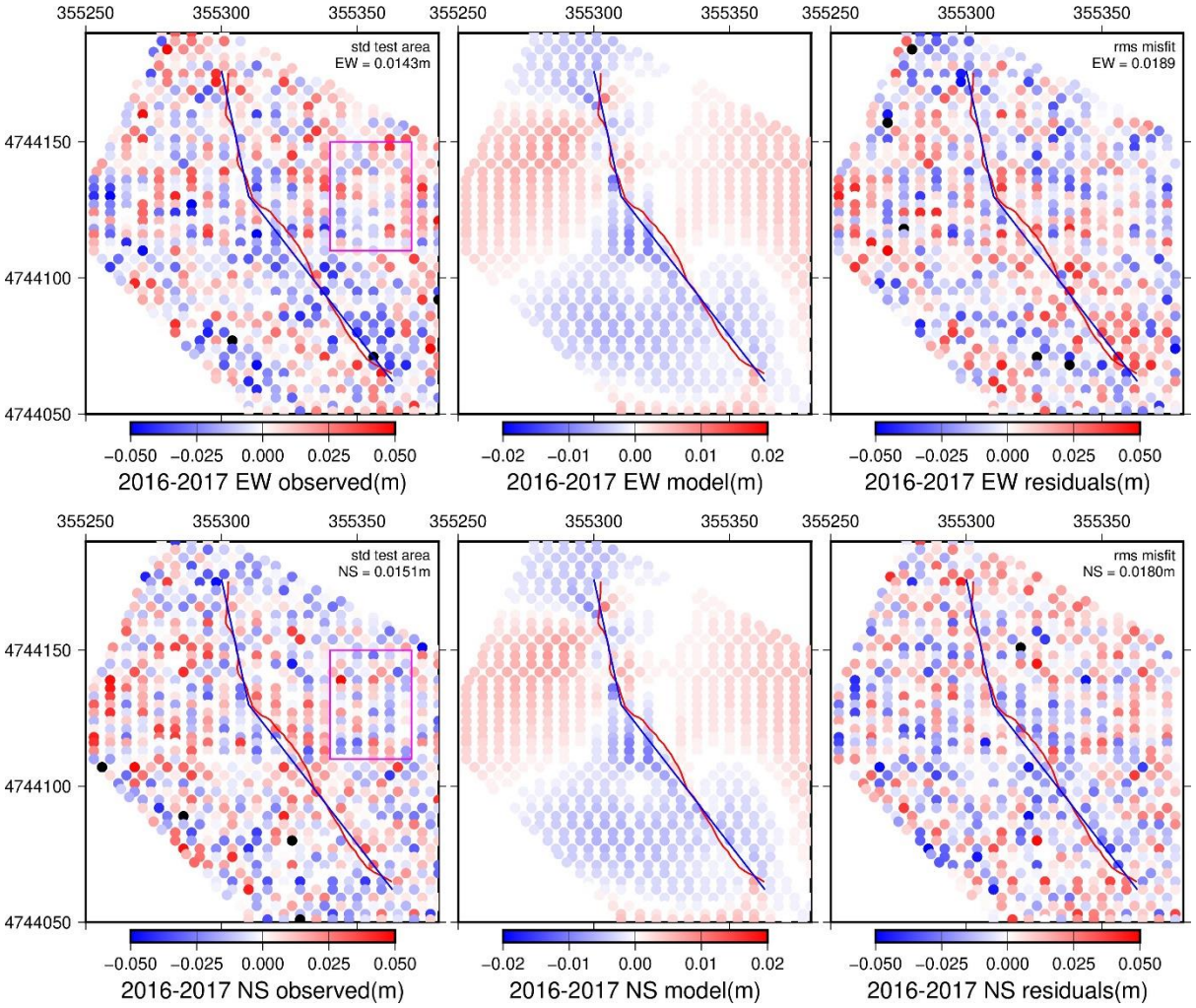

Appendix 4

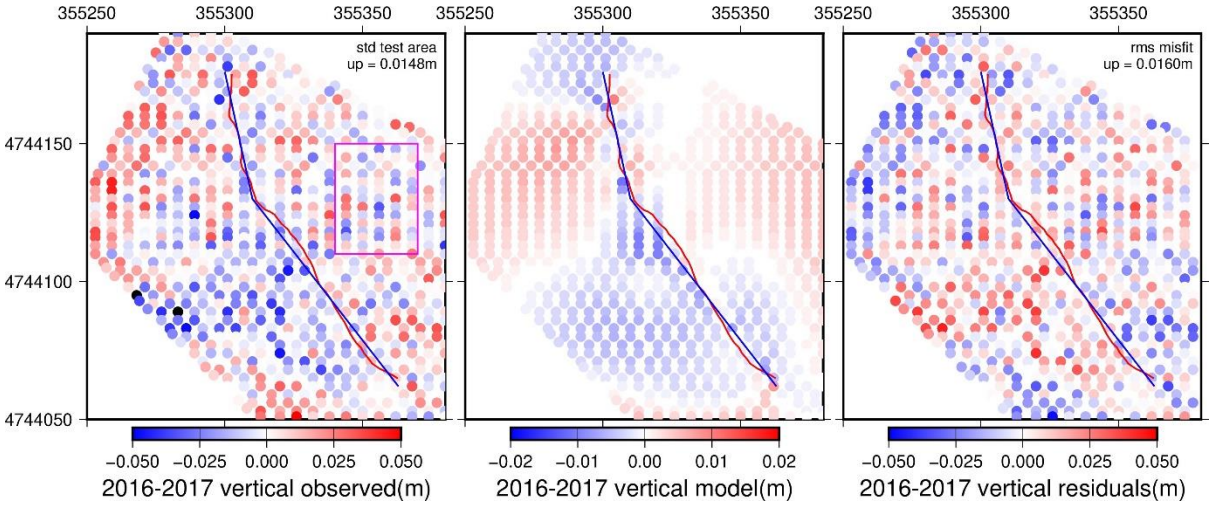

2017-2019

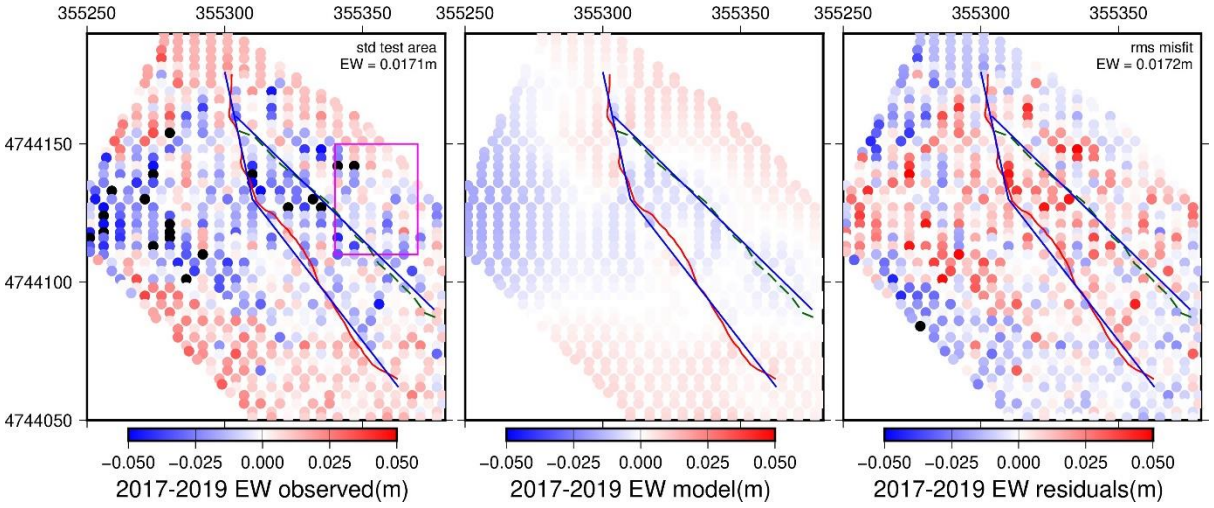

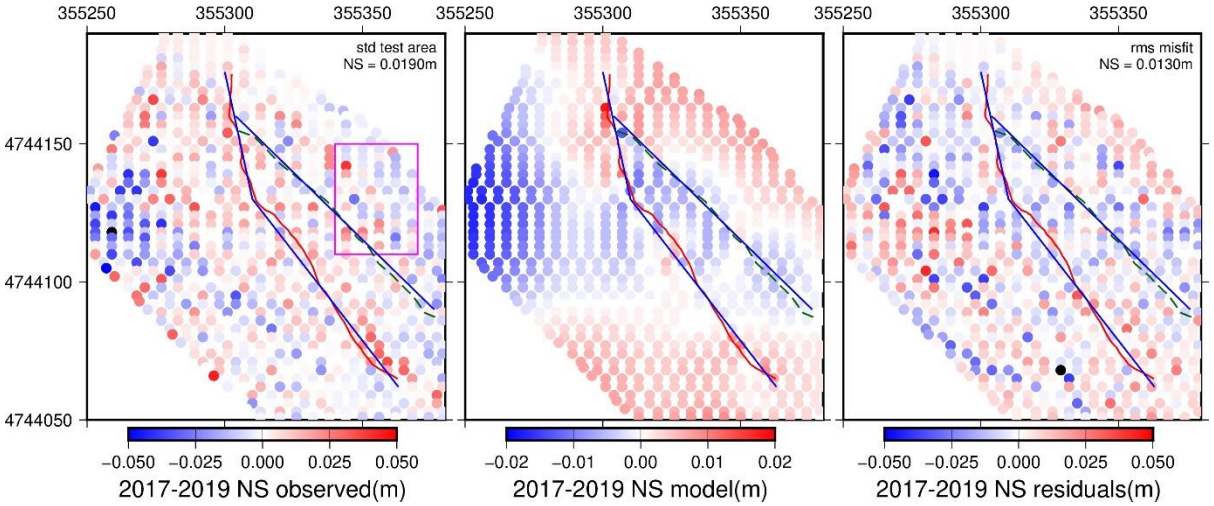

Appendix 4

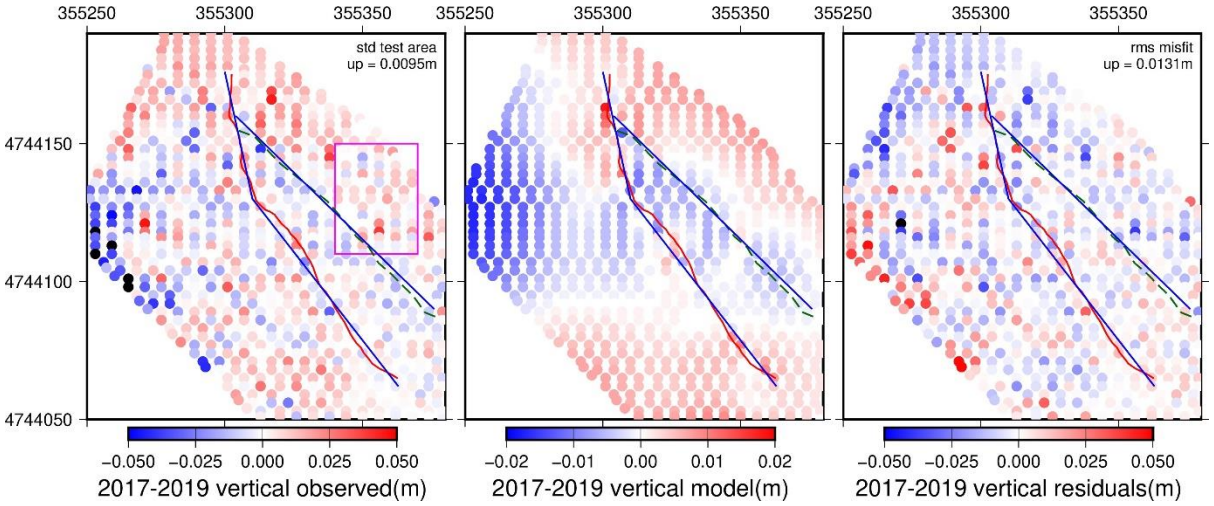

2016-2019

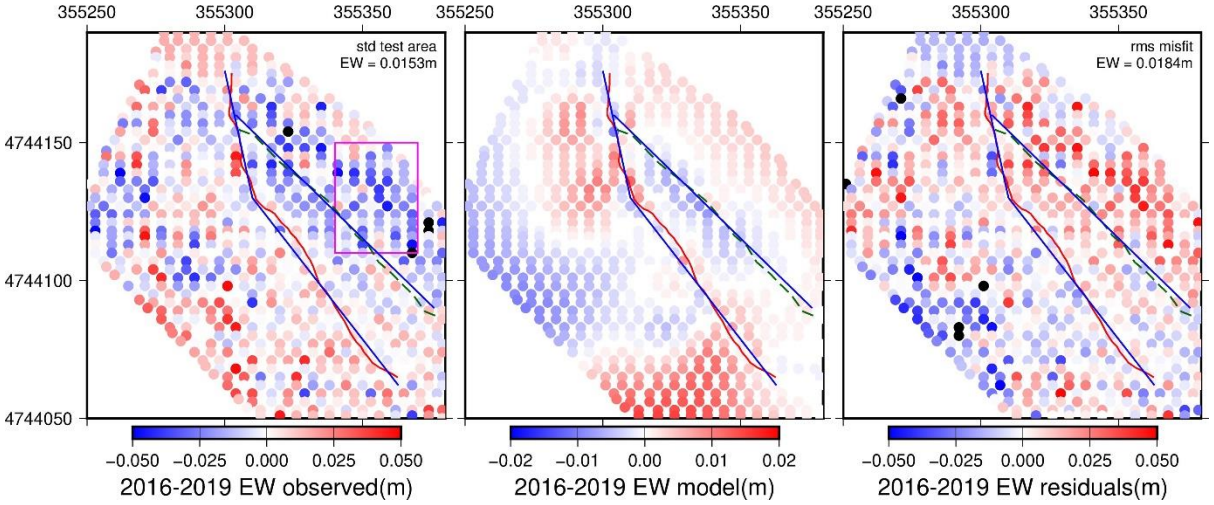

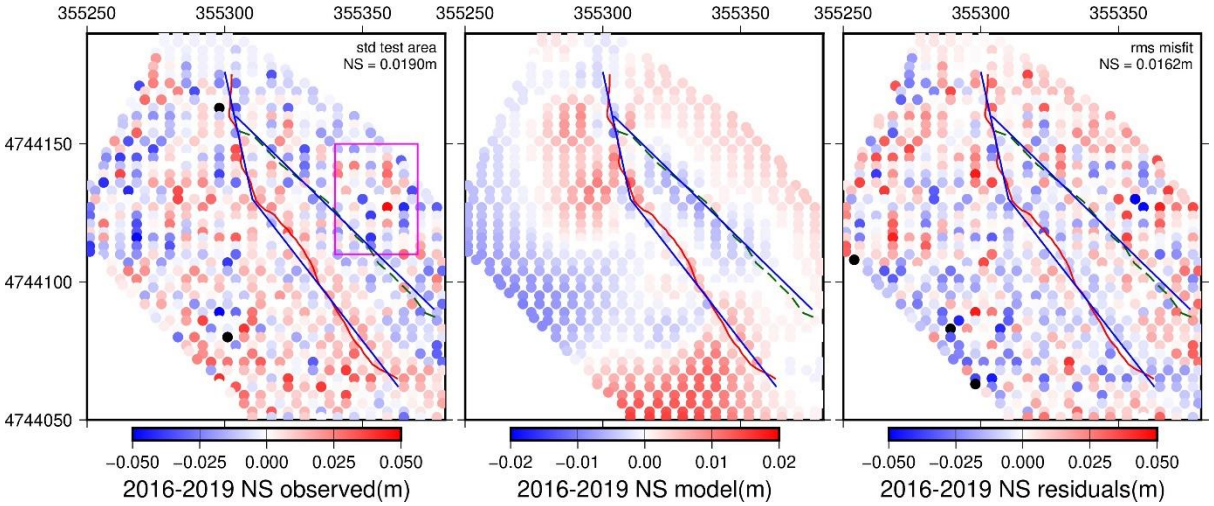

Appendix 4

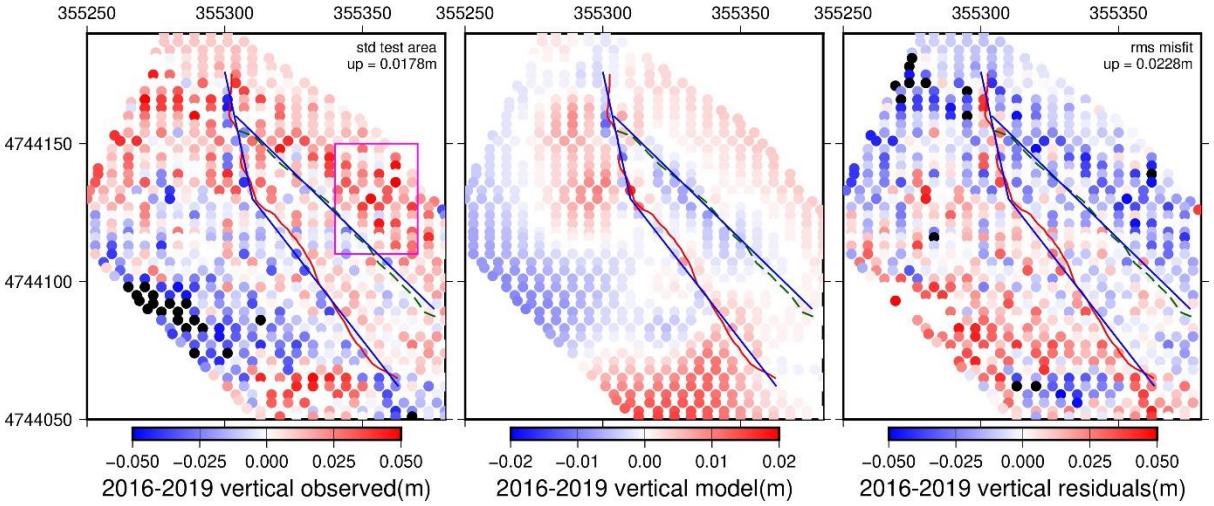
355250
355300
355350
4744150
4744100
4744050
std test area
up = 0.0178m
rms misfit
up = 0.0228m
−0.050 −0.025 0.000 0.025 0.050
2016-2019 vertical observed(m)
−0.02 −0.01 0.00 0.01 0.02
2016-2019 vertical model(m)
−0.050 −0.025 0.000 0.025 0.050
2016-2019 vertical residuals(m)

Part 4.2 Meterff site photographs from May 2022

1. Scarp deterioration

The photographs start with an overview then show the scarp in descending height order

Overview of scarp and hanging wall debris from alluvial channel, looking NE

Appendix 4

NW end of scarp study site, looking NW

Appendix 4

Area of greatest co-seismic recorded slip, looking NE

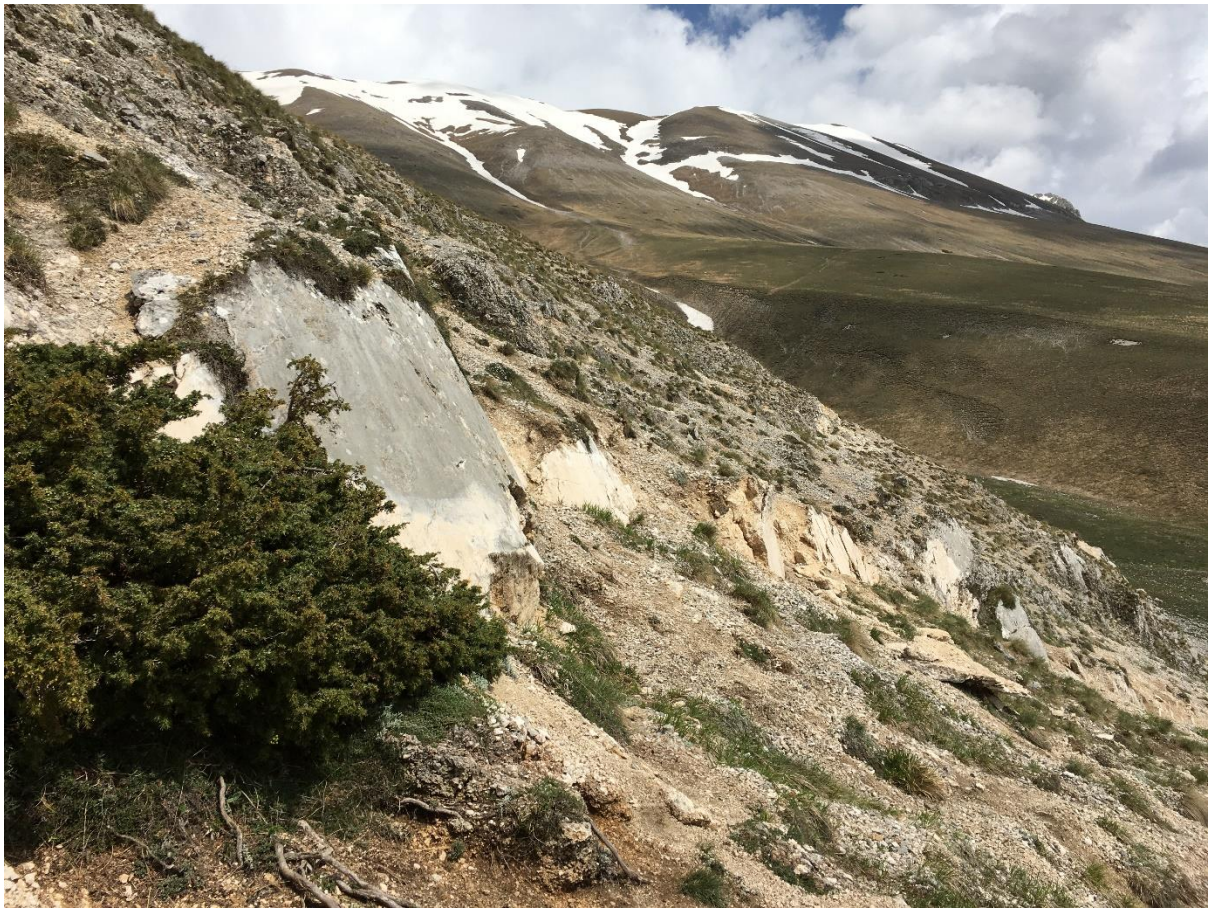

View from previous location down scarp line, looking SE

View further down scarp line, looking SE

Fractured and eroding sections of scarp towards SE end of site, looking N towards previous photograph

Eroded section of scarp towards SE end of site, and debris in hanging wall, looking SE

Debris along scarp line at furthest SE end of site, looking N

Appendix 4

Debris in alluvial channel, looking ESE

2. Hanging wall and alluvial fan debris

Debris in alluvial channel, looking W

Debris in lower part of hanging wall, looking ENE

Debris in footwall and hanging wall, taken from footwall above area of largest co-seismic displacement, looking SW across alluvial channel

Appendix 4

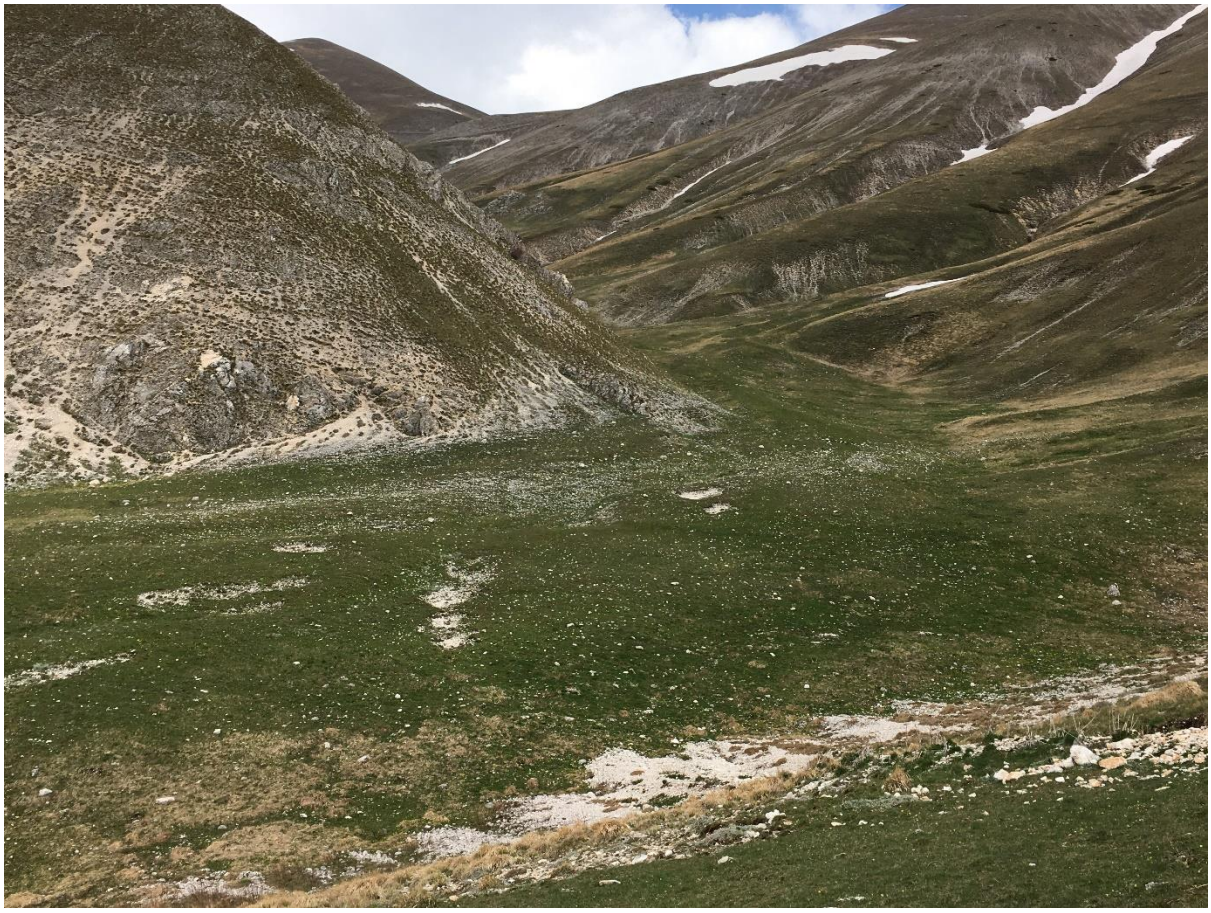

Debris in alluvial channel, looking NE

3. Erosion of footwall

Footwall bedrock with eroded sections, looking SE

Appendix 5

Footwall bedrock with eroded sections and extensive small-scale debris, looking SE

Appendix 5

Footwall bedrock with eroded sections above area of largest co-seismic displacement, looking NW

Appendix 5

Footwall bedrock with eroded sections and extensive small-scale debris, looking NW taken from above midpoint in the fault scarp

Appendix 5

Footwall bedrock with eroded sections and extensive small-scale debris, looking SE taken from above midpoint in the fault scarp

APPENDIX 5

Part 5.1. Individual slip components by TLS site, before filtering and/or detrending

5.1(a) Vettore Antithetic 1

(Detrended results before filtering)

2016-2017

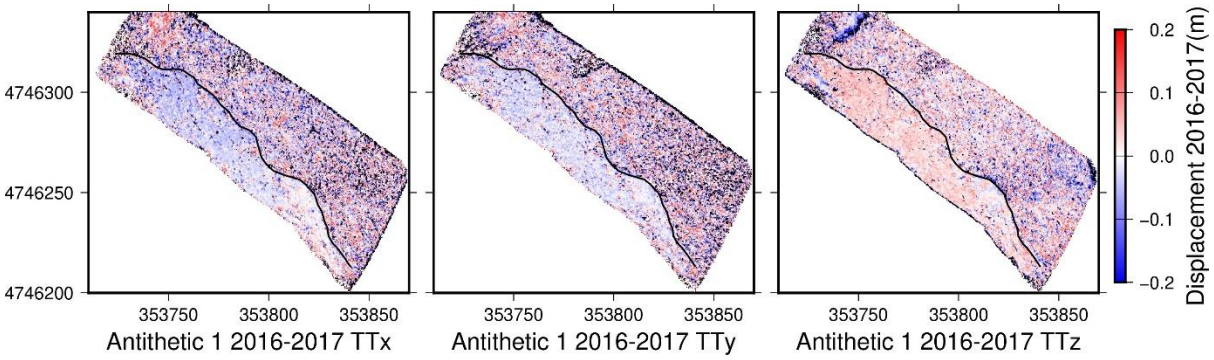

2017-2019

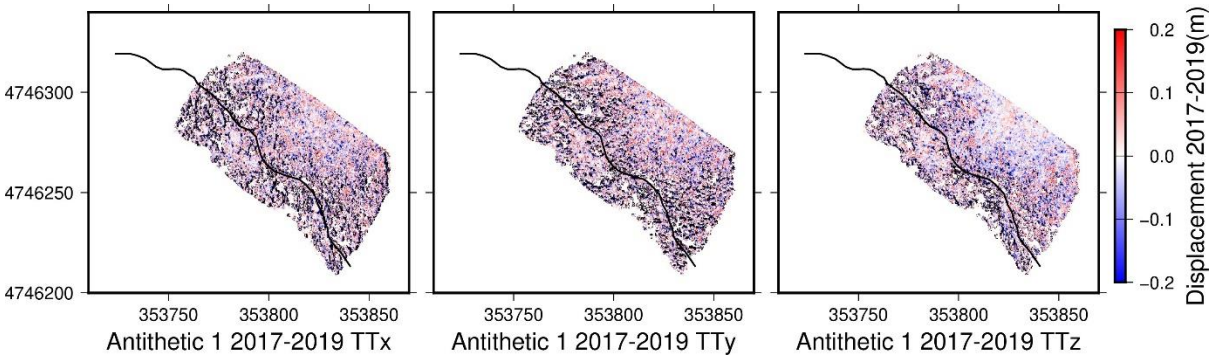

2016-2019

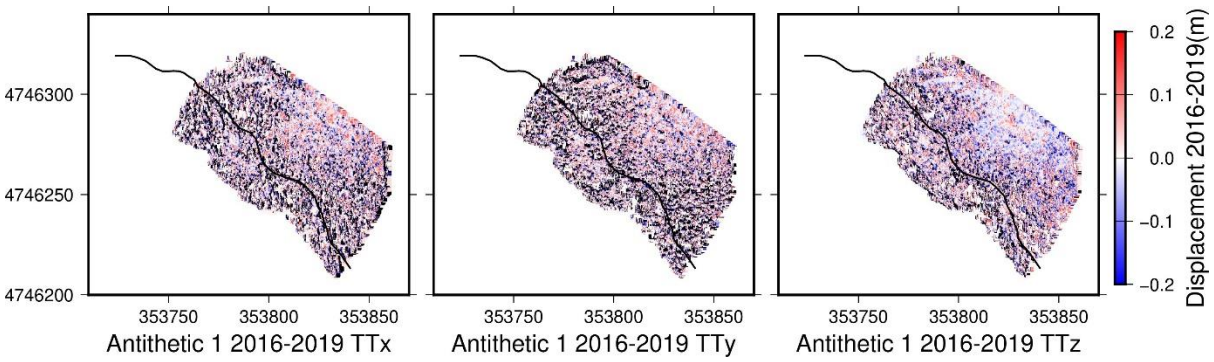

5.1(b) Vettore Road

2016 (Oct) – 2016 (Nov)

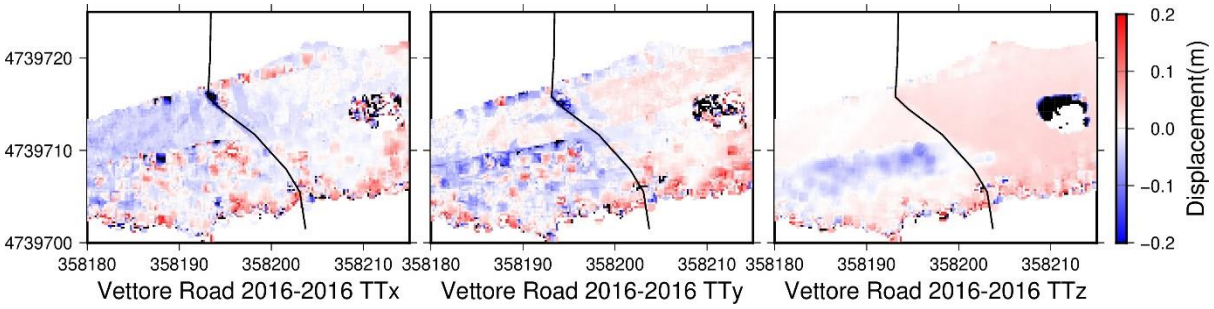

2016 (Oct) - 2017

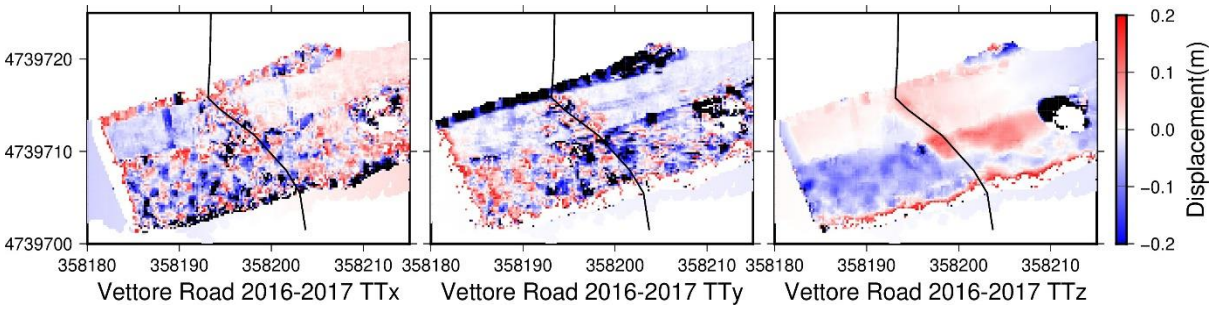

2016 (Nov) – 2017

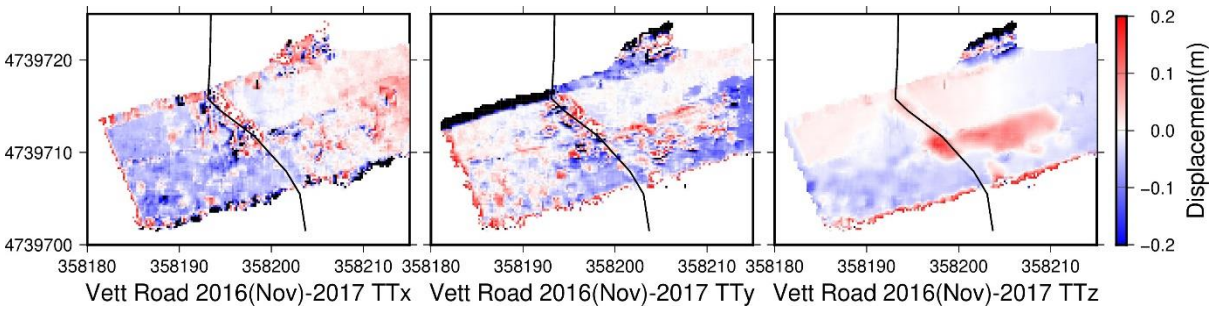

2017 - 2019

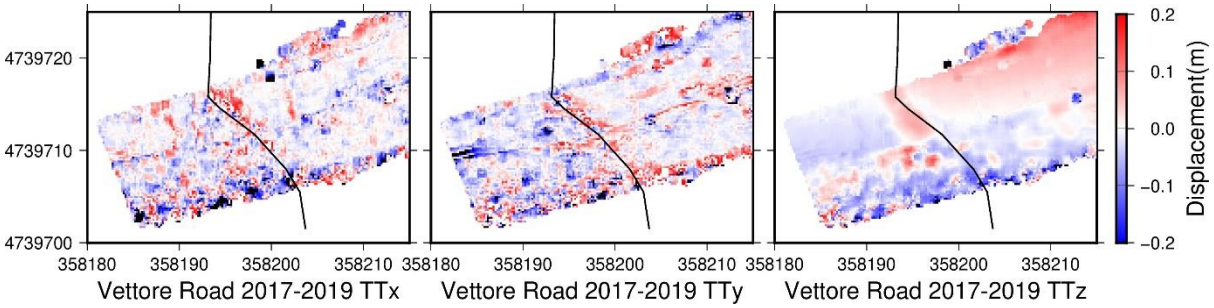

Part 5.2. TLS site field photographs from May 2022

5.2(a) Vettore Antithetic 1 site

1. Views of sub-vertical outcrop, debris in hanging wall below the crag, and deterioration of the scarp in that area

View from hanging wall looking SE towards sub-vertical outcrop

Appendix 5

Hanging wall debris below outcrop, looking SW

Appendix 5

Scarp area of outcrop and debris in hanging wall, looking SW

Appendix 5

Scarp area of outcrop with newly exposed surfaces , looking SW

Scarp area at foot of outcrop, looking S

2. Views of scarp to the NW of the sub-vertical outcrop, and debris in the hanging wall below that part of the scarp

Appendix 5

Debris in hanging wall to NW of outcrop, plus scarp, looking NW.

Detail of debris in hanging wall below scarp to NW of outcrop, pencil for scale

Appendix 5

Debris below central area of scarp, with deteriorating scarp, looking W

Appendix 5

Deteriorating scarp towards NW of study site, looking NW

5.2(b) Castelluccio Road site

View across road, looking NNE, ploughed fault scarp area

Detail of previous view, looking NNE

Appendix 5

View from footwall side, looking NNW

Appendix 5

Resurfaced road, looking W

5.2(c) Vettore Road site

Resurfaced road and hillside protection, looking W

Appendix 5

Cracks in slope on hanging wall side, looking W

Appendix 5

Cracks in slope on footwall side, looking ENE

Appendix 5

Renewed banking further W

Appendix 5

Overview of site looking E

Appendix 5

Hillside protection, looking N

Appendix 5

View of site from distance, showing scarp in hillside, looking E

5.2(d) Bove Road site

1. Fault scarp

Gravel access track, looking S across line of 2016 rupture

Appendix 5

Scarp area in hillside, looking along scarp line towards NE

Appendix 5

Small scale debris below eroding scarp, looking NE

Detail of scarp deterioration and hanging wall debris (pencil for scale)

2. Accumulation of larger debris in hollow in hanging wall

View from scarp line towards area of accumulation in dip in hanging wall, looking SSE

Appendix 5

Accumulated blocky debris in hanging wall dip, pencil for scale

Exposed fractured bedrock in hanging wall above dip, looking up slope towards ENE

Exposed fractured bedrock in hanging wall above dip, looking up slope towards E